THE JOURNAL OF PHYSICAL CHEMISTRY C

Article

pubs.acs.org/JPCC

Efficiency of Interfacial Electron Transfer from Zn-Porphyrin Dyes into TiO_2 Correlated to the Linker Single Molecule Conductance

Christian F. A. Negre,[†,‡] Rebecca L. Milot,[†] Lauren A. Martini,[†] Wendu Ding,[†] Robert H. Crabtree,*[,†,‡] Charles A. Schmuttenmaer,[†,‡,*] and Victor S. Batista*[,†,‡]

[†]Department of Chemistry, Yale University, 225 Prospect St., P.O. Box 208107, New Haven, Connecticut, 06520-8107 United States

[‡]Energy Sciences Institute, Yale University, P.O. Box 27394, West Haven, Connecticut, 06516-7394 United States

Supporting Information

ABSTRACT: High performance dye-sensitized solar cells (DSSCs) rely upon molecular linkers that allow efficient electron transport from the photoexcited dye into the conduction band of the semiconductor host substrate. We have studied photoinduced electron injection efficiencies from modular assemblies of a Zn-porphyrin dye and a series of linker molecules which are axially bound to the Zn-porphyrin complex and covalently bound to TiO_2 nanoparticles. Experimental measurements based on terahertz spectroscopy are compared to the calculated molecular conductance of the linker molecules. We find a linear relationship between measured electron injection efficiency and calculated single-molecule conductance of the linker employed. Since the same chromophore is used in all cases, variations in the absorptivities of the adsorbate complexes are quite small and cannot account for the large variations in observed injection efficiencies. These results suggest that the linker single-molecule conductance is a key factor that should be optimized for maximum electron injection efficiencies in DSSCs. In addition, our findings demonstrate for the first time the possibility of inferring values of single molecule conductance for bridging molecules at semiconductor interfaces by using time-resolved THz spectroscopy.

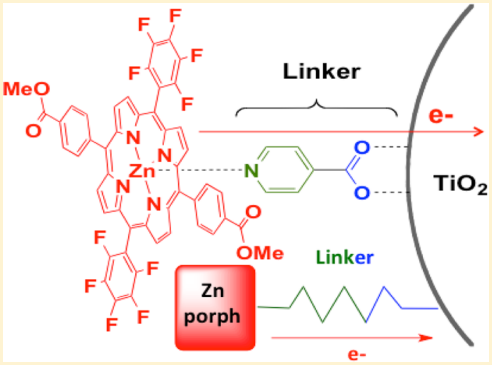

1. INTRODUCTION

Ever since the seminal work of O'Regan and Grätzel,[1] dye-sensitized solar cells (DSSCs) have continued to raise significant interest as promising alternatives for solar-to-electric energy conversion. DSSCs are particularly attractive since they are based on inexpensive semiconductor materials (typically nanoporous TiO_2, ZnO, or SnO_2)[2−5] sensitized to visible light absorption with dyes covalently attached to the semiconductor surface by molecular linkers. Photoexcitation of the sensitizer dye leads to electron−hole pair separation, injecting electrons through the molecular linkers into the conduction band (CB) of the semiconductor surface. The photogenerated electron carriers then flow through the external load toward the cathode, performing useful electrical work along the way. At the cathode, electrons reduce a redox mediator (e.g., I_3^-), generating a redox species (e.g., I^-) which refills the holes left behind on the sensitizer molecules.[2,6] While significant research effort has been devoted to the study of DSSCs, the outstanding challenge is to improve the photoconversion efficiency. Here, we focus on the transport properties of the molecular linkers as directly correlated to the efficiency of electron injection into the semiconductor.

A variety of dyes for DSSCs have been explored beyond the initially utilized Ru−polypyridyl complexes, including inexpensive alternatives such as π-conjugated organic molecules that bypass the need of precious metals.[7−11] These organic dyes are promising because they exhibit large $\pi-\pi^*$ excitation cross sections and absorb strongly in the visible region of the spectrum.[12−18] Organic DSSCs with efficiencies up to 11% have been prepared very recently.[19] Zn-porphyrin dyes, which have been incorporated in some of the most efficient DSSCs to date,[20,21] are particularly attractive since they have high molar absorptivity. In addition, the spectral and electronic properties can be tuned by varying both the centrally coordinated metal ion and the peripheral substituents.[22−24] Metal porphyrins can bind directly to the semiconductor surface via built-in anchoring groups at the beta- and meso-positions or alternatively through linkers that coordinate to the metal center in the axial position (Figure 1a).[25−28] The advantage of the axial binding motif is that it separates the design and synthesis of the linker from the development of the porphyrin dye, thereby simplifying the design of the chromophore/redox active center and assembly of the molecular framework to the semiconductor surface. Nevertheless, axial linkers have been much less investigated, compared to anchoring groups substituting at the beta or meso positions of the porphyrin ring. It is therefore important to analyze the efficiency of photoinduced electron injection as a function of the linker structure[25] and explore structure/function relations that might

Received: August 31, 2013
Revised: October 21, 2013
Published: October 23, 2013

   dx.doi.org/10.1021/jp408738b | J. Phys. Chem. C 2013, 117, 24462−24470

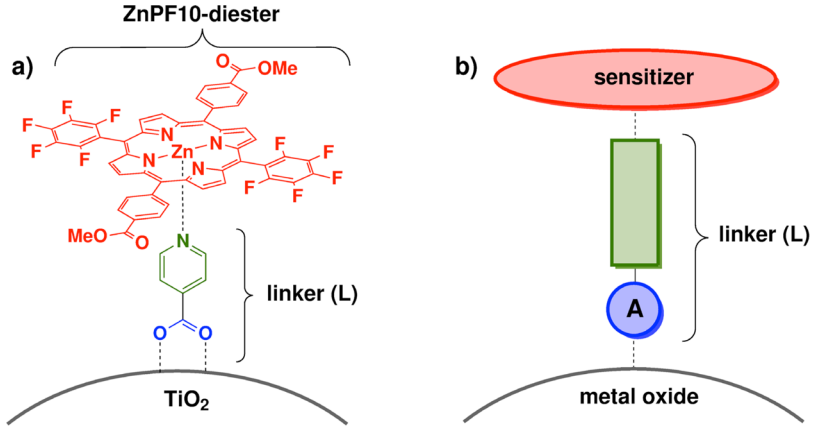

Figure 1. (a) $ZnPF_{10}$-diester bound to TiO_2 via a pyridyl linker using the modular assembly technique. (b) Cartoon depiction of the modular assembly method for attaching Zn porphyrins to TiO_2 via simple molecular linkers with varying anchor groups. The porphyrin sensitizer, linker (L), and anchors (A) are described in the text.

correlate the resulting interfacial electron transfer efficiency with the electrical properties of the linkers.

High-potential porphryin dyes have been assembled in photoanodes for DSSCs[29] as well as in photocatalytic cells for light-driven water splitting when codeposited with a water oxidation catalyst on TiO_2 thin films.[30] They were found to be quite versatile since they could be optimized to give sufficiently positive redox potentials, as necessary to activate catalysts for water oxidation. Furthermore, when covalently bound to semiconductor surfaces, they were stable under oxidative and aqueous conditions, as necessary for photocatalytic water oxidation. However, the reported cells have shown low efficiency calling for fundamental studies of the factors responsible for efficiency loss.

In addition to the optimization of the spectral and electrochemical properties of the dye, optimum performance requires assemblies that maximize electron injection into the semiconductor.[31−35] For metal-porphyrins bound through axial coordination, electron injection can be optimized through suitable design and refinement of the molecular linker.[36] Two photoinjection mechanisms are possible: photoexcitation of the dye, followed by injection through the molecular linker (type-I), or direct injection from the ground state of the dye to the CB of the semiconductor (type-II).[37−40] While both mechanisms involve ultrafast time scales,[41,42] the type-I process is usually favored in porphyrin dyes as well as in the molecular assemblies most commonly used in DSSCs.[43] Therefore, it is important to focus on optimization of interfacial electron injection by design of molecular linkers that provide proper alignment of electronic states and strong electronic coupling with the semiconductor CB.

Several experimental techniques have been used to study photoinjection mechanisms in DSSCs and to determine the efficiency and time scales of interfacial electron transfer at a variety of semiconductor surfaces, including transient absorption spectroscopy, electron paramagnetic resonance, and time-resolved terahertz (THz) spectroscopy.[5,44−50] In addition, analytical studies and computational simulations of interfacial electron transfer have advanced our understanding of the complex interrelation between the dye and the semiconductor surface.[23,40,51−59] These studies have shown that highly conductive linkers, such as molecular frameworks with conjugated double bonds, usually inject carriers much faster than aliphatic linkers. In addition, several studies have focused on the differences in electron injection observed for different anchoring groups.[25,60−63] However, a systematic study of the molecular origin of differences in the efficiency of interfacial electron injection has yet to be reported. In this work, we employ a series of modular linker-porphyrin assemblies that vary in their anchoring group for surface attachment. We find that the efficiency of interfacial electron injection as probed by THz spectroscopy correlates with the single molecule conductance of the linkers binding Zn-porphyrin dyes to TiO_2 surfaces. The resulting insight is particulary relevant to the design of linker-porphyrin assemblies when combined with optimization of photoabsorption and redox properties by inverse design techniques.[36] These findings also demonstrate for the first time the possibility of inferring values of single molecule conductance by using time-resolved THz spectroscopy for molecules bridging electron donor adsorbates at semiconductor interfaces.

2. EXPERIMENTAL AND COMPUTATIONAL METHODS

2.1. Sample Preparation. All compounds were obtained or synthesized from commercially available starting materials and were used without further purification unless otherwise noted. Isonicotinic acid (L1) and 4-pyridyl-boronic acid (L5) were obtained from Aldrich. The molecular linkers 4-pyridyl-phosphonic acid (L2), 4-pyridyl-acetylacetonate (L3), and 4-pyridyl-hydroxamic acid (L5) were synthesized according to a previously reported literature procedure.[64−68] The high-potential zinc porphyrin dye $ZnPF_{10}$-diester was also synthesized according to a previously reported literature procedure.[29,30]

Mesoporous thin films of TiO_2 were prepared using Degussa Aeroxide P25 titanium dioxide nanoparticles by either doctor-blading or spin-coating. Films used for absorbance measurements were prepared on microscope coverslips (25 × 25 mm for spin-coating, 22 × 50 mm for doctor-blading, Fisherbrand, USA). Films used for time-resolved THz spectroscopy measurements were prepared on fused quartz microscope slides (1 × 1 in, 1 mm thickness, GM Associates, Inc., USA). Bare TiO_2 thin films were soaked overnight in the dark in a 0.5 mM solution of the desired linker (L1-L5) in ethanol and thoroughly rinsed with ethanol to remove unbound linker. The films were dried at room temperature for at least 30 min, soaked overnight in the dark in a 0.1 mM dichloromethane solution of the $ZnPF_{10}$-diester porphyrin, and rinsed well with

dx.doi.org/10.1021/jp408738b | J. Phys. Chem. C 2013, 117, 24462−24470

dichloromethane to remove any uncoordinated or aggregated porphyrin.

Absorption spectra were recorded using a Cary 3E UV−visible spectrophotometer (Agilent Technologies). Thin films of TiO_2 were highly scattering so absorbance spectra of all thin films were taken in diffuse reflectance geometry using an integrating sphere attachment.

2.2. Time-Resolved THz Spectroscopy (TRTS) Measurements. An amplified Ti:sapphire laser (Tsunami/Spitfire from Spectra Physics) generated 800 mW of pulsed near-IR light at a 1 kHz repetition rate. The pulse width was ∼130 fs, and the center wavelength was 800 nm. Roughly two-thirds of the power was frequency doubled and then filtered to produce 40 mW of 400 nm (3.1 eV) light for the pump beam. The remainder of the near-IR light was used to generate THz radiation via optical rectification in a ZnTe(110) crystal and detect it using free space electro optic sampling in a second ZnTe(110) crystal. Terahertz data were taken at room temperature, and the average of two samples was taken for each data set. Further information on the spectrometer and technique can be found in the literature.[45,69−71]

2.3. Conductance and Electronic Structure Calculations. The steady state current flowing through the molecular linker has been computed according to the Landauer−Büttiker formula[72,73]

$$I = \frac{2e}{h}\int_{\mu_L}^{\mu_R} T(E)\,\mathrm{d}E \tag{1}$$

where e is the electron charge, h is Planck's constant, μ_L and μ_R are the chemical potentials for the electron in the left and right leads, respectively (Figure 2), and E is the energy of the conducting channel. The transmission function T is calculated by using the Fisher−Lee formula[74]

$$T = Tr(g^{+}_{dev}(E)\Gamma_L(E)g^{-}_{dev}(E)\Gamma_R(E)) \tag{2}$$

where $g^{+}_{dev}(E)$ is the advanced nonequilibrium Green's function (NEGF) operator for the system consisting of the device attached to one-dimensional leads, as shown in Figure 2.[75]

The NEGF operator can be written, as follows:

$$g_{dev}(z) = (zS - H_{dev} - \Sigma_L(z) - \Sigma_R(z))^{-1} \tag{3}$$

where z is the generalized complex energy variable, S is the overlap matrix, H_{dev} is the Hamiltonian of the molecule, and Σ_L and Σ_R are the self-energy operators corresponding to the left and right leads, respectively. Γ is defined as follows:

$$\Gamma_{L/R} = i(\Sigma^{+}_{L/R}(E) - \Sigma^{-}_{L/R}(E)) \tag{4}$$

where $\Sigma^{+}_{L/R}(E)$ and $\Sigma^{-}_{L/R}(E)$ are the advanced and retarded self-energy operators for the left (L) and right (R) contacts, respectively.

The electronic structure and transport properties of the linkers were determined by using the semiempirical extended-Hückel (EH) Hamiltonian in conjunction with the NEGF methodology.[76−78] In the basis of localized atomic orbitals, the matrices $\Sigma_{L/R}$ are assumed to be diagonal with nonzero elements $(\Sigma_{L/R})_{11} = \gamma^2 g_0^{+L}(E)$ and $(\Sigma_{L/R})_{NN} = \gamma^2 g_0^{+R}(E)$ where the indices $1 - N$ label the atomic orbitals of the linker that have significant overlap with the left and right leads. The parameter γ defines the effective electronic coupling with the contacts and is assumed to the same for s, p, and d orbitals. The Green's function for the isolated left and right contacts, $g_0^{+L/R} = -i/|\beta|$, are defined to mimic semi-infinite one-dimensional nanowires as described by a nearest-neighbor tight-binding Hamiltonian with constant intersite coupling β.[79] The value of $\gamma^2/|\beta| = 2.0$ eV was chosen to ensure that the conductance of a linear chain of gold atoms at 0 V bias is equal to the unit of quantum conductance (i.e., $G_0 = 2e^2/h$) when connected to the model nanowire leads, as recently reported.[78] All calculations of conductance were performed at 0 V bias. Hence

$$G = \frac{2e^2}{h}T(E_F) \tag{5}$$

where G is the molecular conductance (in Siemens), and the transmission function T is evaluated at the device Fermi level E_F. The geometries of the linkers (Figure 3) correspond to optimized minimum energy configurations, obtained via density functional theory (DFT) at the B3LYP/LANL2DZ level, as implemented in Gaussian 09.[80]

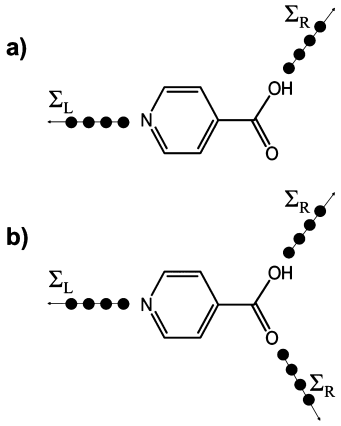

Figure 2. Scheme depicting the coupling of 4-pyridyl-carboxylic acid to the semi-infinite leads in monodentate (a) and bidentate (b) binding motifs.

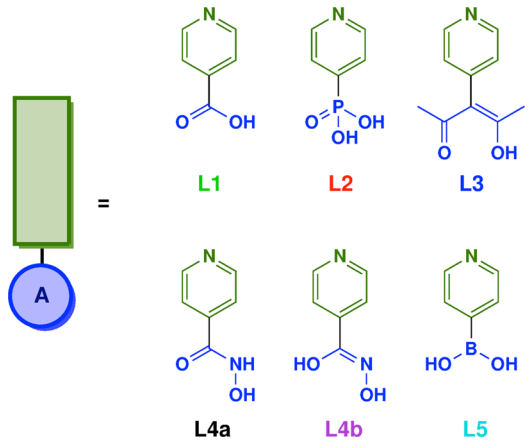

Figure 3. Linker molecules (L) substituted with different anchoring groups (A) that covalently bind Zn-porphyrin sensitizers to TiO_2 surfaces. Linkers have the structure 4-pyridyl-A, where the anchoring group A is either carboxylic acid (L1), phosphonic acid (L2), acetylacetonate (L3) hydroxamic acid (L4), or boronic acid (L5).

dx.doi.org/10.1021/jp408738b | J. Phys. Chem. C 2013, 117, 24462−24470

3. RESULTS AND DISCUSSION

Figure 3 shows the structures of the linkers analyzed in this study. All the linkers have the form 4-pyridyl-A where the anchoring group A is either carboxylic acid (L1), phosphonic acid (L2), acetylacetonate (L3), hydroxamic acid (L4), or boronic acid (L5). Hydroxamic acid is treated in both of its two tautomers L4a and L4b.[81] These anchoring groups are known to bind strongly to semiconductor surfaces while the pyridyl group axially coordinates to the metal center of the prophyrin $ZnPF_{10}$ through the pyridyl nitrogen, sensitizing the TiO_2 surface (Figure 1).[82] These surface-bound complexes are collectively denoted L-$ZnPF_{10}$, with L = L1−L5.

Figure 4 shows the UV−vis diffuse reflectance spectra of the L-$ZnPF_{10}$ assemblies bound to TiO_2 showing only small differences in the molar absorptivity of the chromophore-linker assemblies. In fact, Figure 4 shows that L1-$ZnPF_{10}$, L2-$ZnPF_{10}$, and L4-$ZnPF_{10}$ have nearly the same absorbance at around 400 nm, which is the wavelength of the pump pulse in our THz measurements, while the absorptivities of L3-$ZnPF_{10}$ (shown) and L5-$ZnPF_{10}$ (not shown) are only slightly lower. Therefore, differences in the observed photoinjection yields of these assemblies cannot be attributed to differences in light-harvesting efficiency.

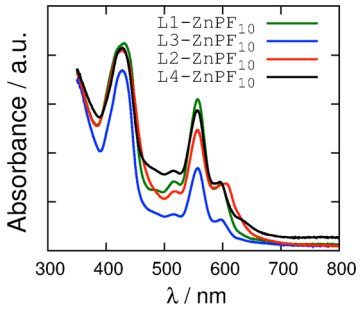

Figure 4. Experimental UV−vis diffuse reflectance spectra for L-$ZnPF_{10}$ complexes covalently bound to nanoporous TiO_2 thin films.

Figure 5 shows the change in transmitted THz amplitude as a function of time after the TiO_2 thin-films sensitized with L-$ZnPF_{10}$ are photoexcited with a pump pulse at 400 nm. The attenuation of THz amplitude is a measure of the efficiency of electron injection, since it is proportional to the concentration of free charge carriers injected into the semiconductor conduction band (denoted state *B* in Figure 6).[45,71,83,84] As a control experiment, we note there is no detectable attenuation of THz transmittance when $ZnPF_{10}$ is merely physisorbed on the TiO_2 surface, whereas all of the L-$ZnPF_{10}$ complexes covalently bound to the surface show measurable attenuation. We also performed a seccond control experiment that shows no injection from porphyrin-free L1-sensitized anatase compared to the full system (L1-$ZnPF_{10}$; see Figure S4). Since the predominant porphyrin excitation near 400 nm (the Soret or B band) arises from the $S_2 \leftarrow S_0$ transition, which is $\pi^* \leftarrow \pi$, these results suggest that the photoinjected carriers must travel through the linkers (or through space) in order to be injected into TiO_2. From the THz data alone, however, we see significant differences in the efficiency of electron injection for the different anchoring groups. The efficiencies of electron injection for the various L-$ZnPF_{10}$ complexes can be ranked according to the order: L4 > L1 > L2 ≈ L3 ≈ L5.

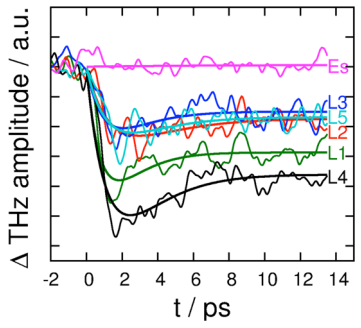

Figure 5. Change in THz amplitude (thin lines) measured as a function of time after photoexcitation at 400 nm for L-$ZnPF_{10}$ assemblies covalently bound to TiO_2 surfaces as shown in Figure 1. Thick lines are best fitting curves determined by the kinetic model described in the text (eq 6). As a control, the magenta corresponds to $ZnPF_{10}$-diester (Es) physisorbed to the TiO_2 surface in the absence of a molecular linker.

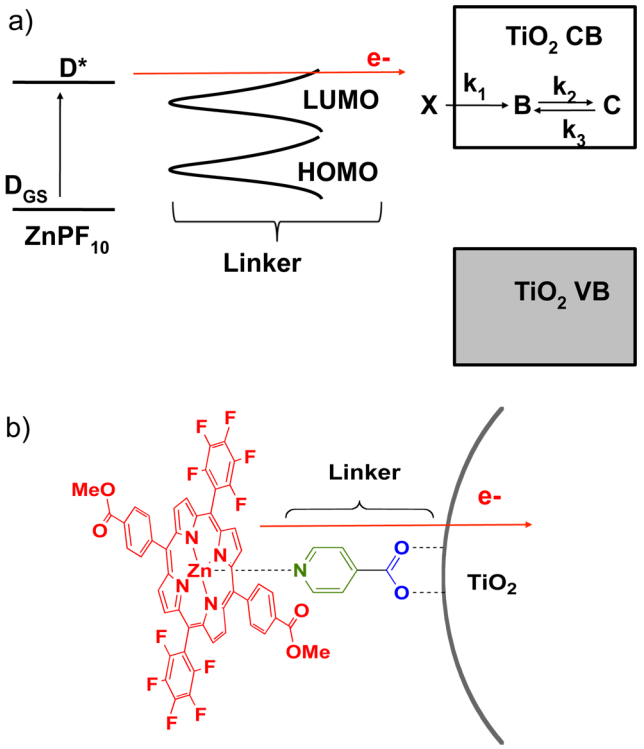

Figure 6. Schematic diagram of photoinjection in terms of the most relevant energy levels (a) and molecular structures (b). D_{GS} and D* correspond to the porphyrin dye $ZnPF_{10}$ in the ground (S_0) and second excited state (S_2), respectively. *X* represents the carrier concentration at the TiO_2 surface prior to injection, *B* is the concentration of free carriers injected into the TiO_2 conduction band, and *C* is the concentration of trapped carriers.

Figure 6 shows a schematic diagram of the photoinjection process. Upon photoexcitation of the dye, electrons are transferred through the pyridyl ligand and anchoring group to the semiconductor surface (D* → X). This is an ultrafast[51] electron transmission process that takes a few femtoseconds prior to the interfacial injection of free carriers into the conduction band (X → B with an injection rate constant k_1 of tens to hundreds of femtoseconds). The kinetic model also includes trapping (B → C) and detrapping (C → B) dynamics with rate constants k_2 and k_3, respectively. According to this

dx.doi.org/10.1021/jp408738b | J. Phys. Chem. C 2013, 117, 24462−24470

kinetic model, the concentration of free carriers B, as a function of time t, is given by the following equation:

$$B(t) = X_0(\theta_1 + \theta_2 e^{-k_1 t} + \theta_3 e^{-(k_2+k_3)t}) \quad (6)$$

where

$$\theta_1 = \frac{k_3}{k_2 + k_3}$$

$$\theta_2 = \frac{(k_1 - k_3)}{-k_1 + k_2 + k_3}$$

$$\theta_3 = \frac{k_1 k_2}{(k_2 + k_3)(k_1 - k_2 - k_3)} \quad (7)$$

The derivation of eqs 6 and 7 is provided in the Supporting Information (SI). Equation 6 provides a description of the time-dependent concentration of free carriers that should be proportional to the observed attenuation of THz transmitted amplitude for the different anchoring groups. The trapping and detrapping rate constants k_2 and k_3 are assumed to depend only on the nature of the semiconductor and therefore are treated as global fitting parameters common to all anchoring groups. The parameter X_0, which is reported in Table 1 for each linker, gives

Table 1. Calculated Conductance Values (G) for Linkers in Monodentate and Bidentate Binding Modes and the Maximum Change in THz Amplitude X_0[a]

	conductance, $G/10^3$ nS		
linker	bidentate	monodentate	X_0/arb. units
L1	(2.11)	7.26	6.95
L2	(7.90)	3.99	4.56
L3	2.37	(1.16)	3.76
L4-a	13.36	(3.50)	9.31
L4-b	6.27	(2.99)	9.31
L5	(5.77)	2.76	4.29

[a]Bracketed values do not correlate with X_0 since they do not correspond to the proper binding mode of the ligand (bidentate for L3 and L4 and monodentate for L1, L2 and L5).

a measure of the efficiency of photoinjection as probed by THz spectroscopy since it is proportional to the THz amplitude at the time of maximum attentuation, t_m, and therefore proportional to the concentration of electrons injected into the semiconductor conduction band.

For comparison, Table 1 also reports the values of single molecule conductance computed for each linker by using the EH NEGF methodology outlined in section 2.3. Values for L3 and L4 were calculated assuming a bidentate binding mode, while L1, L2, and L5 were assumed to have monodentate binding. The attachment mode (bidentate for L3 and L4 and monodentate for L1, L2, and L5) is determined for each ligand according to the DFT minimum energy configuration (Figure S5, SI). Our results are consistent with the special arrangement of oxygen atoms, separated by more than two bonds in L3 and L4 anchoring groups, leading to a configuration that is more favorable for bidentate binding with Ti^{4+} octahedral sites.[49,50] Monodentate binding is found to be most stable for L1, L2, and L5, consistent with previous reports for L1,[85] L2,[61] and L5.[86,87] Also, crystallographic data for the dyes absorbed onto novel $(TiO_2)_{17}$ clusters shows a bidentate chelating mode for L3.[88]

The case of L4 has been previouselly modeled showing a favorable bidentate oxygen vacancy mode.[50]

The conductance value for L4 was taken as the average between the conductance values for L4a and L4b[81] because the DFT computed energy diference between the two conformers is less than 0.1 eV.

Figure 7 shows the correlation of the maximum change in THz amplitude X_0 as a function of the linker conductance in

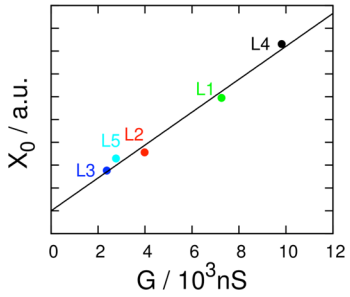

Figure 7. Change in THz amplitude (X_0) at the time of maximum attenuation (t_m) versus conductance G computed for the various linkers. The best linear fit is given by $X_0 = 0.7212G + 1.9943$, with $R^2 = 0.9851$.

the L-$ZnPF_{10}$ complexes. The linear relationship ($R^2 = 0.9851$), suggests that the transport properties of the different linkers have a direct effect on the electron injection and efficiency. The observed correlation between electron injection efficiency and calculated molecular conductance provides a valuable guideline for designing new sensitizers. To understand why different linkers have different values of conductances, we analyze the electronic structure/function relations for the different linkers as correlated to their transport properties.

Figure 8 displays the frontier molecular orbitals of linkers L1 and L3 that are primarily responsible for electron transport.

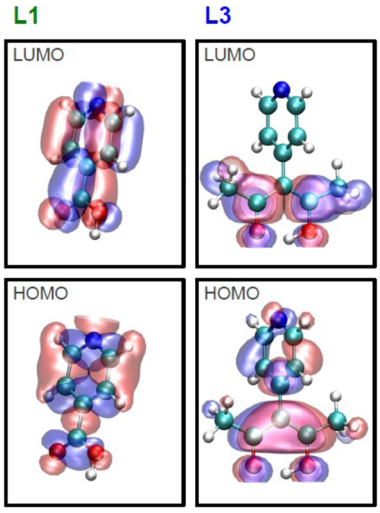

Figure 8. Frontier orbitals calculated within the EH level of theory for L1 and L3.

(Analogous frontier orbitals for L2, L4, and L5 are provided in the SI, Figure S2.) Although L1 and L3 are both known to bind well to the TiO_2 surface,[2,49] L1 has higher conductance and yields much more efficient electron injection than L3. Figure 8 shows that these differences can be attributed to differences in the electronic structure since the pyridine ring of L3 is rotated

dx.doi.org/10.1021/jp408738b | J. Phys. Chem. C 2013, 117, 24462−24470

nearly perpendicularly to the anchoring group and therefore is not conjugated with the electronic structure of the anchor as in L1. Furthermore, the LUMO orbital of L3 is localized on the anchor and therefore does not provide good electronic coupling with the pyridine moiety. In contrast, the LUMO of L1 is delocalized along the entire linker, providing an efficient channel for electron transport.

The analysis of L2 and L5 suggests that phosphonic acid (L2) and boronic acid (L5) functional groups decrease the overall conductance since those functional groups inhibit electron tunneling when bound to the semiconductor surface. In contrast, the hydroxamate linker L4 binds as a bidentate ligand, leading to a more efficient injection than through the monodentate L1 linker.[57] When compared to the bidentate L3 ligand, L4 also leads to much more efficient electron injection due to the extended conjugation and delocalization of the LUMO over the entire linker. EH Frontier orbitals for all the ligands are ploted in Figure S2 in the SI.

The D* → X transport is the primary electron transfer event in porphyrin type-I modular assemblies following photoabsorption at 400 nm due to $\pi^* \leftarrow \pi$ photoexcitation. The photoabsorption and D* → X transport events, however, are dynamically decoupled since the transition dipole moment of the Soret band lies in the plane of the porphyrin ring,[89] which is parallel to the TiO_2 surface. The resulting decoupling with respect to the adiabatic photoinjection[90] is consistent with the observation that the photoabsorption features remain almost unchanged when using linkers with different electron transport efficiency. Figure 9 shows the projected DOS (pDOS) for two

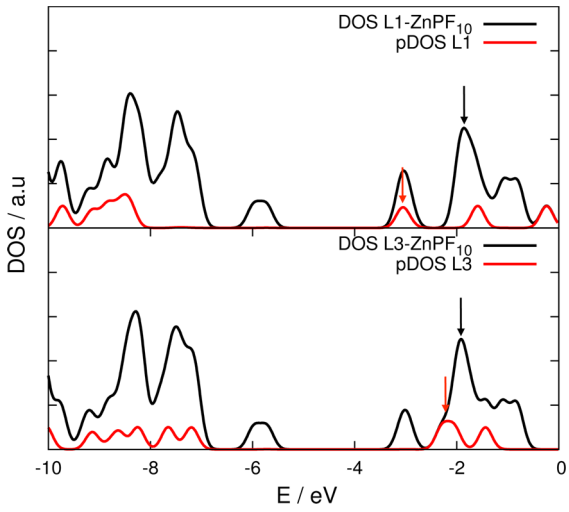

Figure 9. Total density of states (DOS) of the L1-$ZnPF_{10}$ and L3-$ZnPF_{10}$ assemblies (black) and projected DOS onto the linkers L1 and L3 (red). The Fermi level is around −4.44 eV. Red arrows indicating the LUMO for the linker projection. Black arrows indicating the final orbitals participating in the D* → D transition.

of the L-$ZnPF_{10}$ complexes, revealing that the LUMO of the pyridine ligand (red arrows) should be the main orbital responsible for transmission of electrons from the $ZnPF_{10}$ to the conduction band of TiO_2 as it is located right under the porphirin projected excited state (black arrows). DOS for all L-$ZnPF_{10}$ are also shown in Figure S3. These findings suggest that the axial modular assembling technique should be particularly useful for isolating the effect of electron transport properties during electron photoinjection from the photoabsorption properties of the porphyrin dye.

4. CONCLUSIONS

We have studied the efficiency of interfacial electron injection from Zn-porphyrin dyes bound to TiO_2 surfaces via axially coordinated pyridine ligands with a variety of different anchoring groups. The photoconversion efficiency has been characterized by the attenuation of transmitted time-resolved terahertz (THz) signal after photoexcitation and interfacial electron transfer. We found a linear relationship between the interfacial electron injection efficiency and the single molecule conductance of the linker computed according to the nonequilibrium Green's function formalism. This simple relationship suggests that pyridyl linkers in the surface-bound L-$ZnPF_{10}$ complexes function as effective molecular wires, transmitting photoexcited electrons from the light-absorbing porphyrin sensitizer into the conduction band of TiO_2. These results are particularly relevant for optimization of DSSCs that rely upon molecular linkers mediating electron transport from the dye into the conduction band of the semiconductor host substrate. In addition, these findings demonstrate for the first time the possibility of inferring values of single molecule conductance by using time-resolved THz spectroscopy to probe bridging molecules that covalently bind dyes to semiconductor surfaces, while keeping constant the other components of the molecular assembly, such as the nature of the dye and the semiconductor material.

■ ASSOCIATED CONTENT

Ⓢ Supporting Information

Kinetic model and derivation of eq 6; additional figures with the analysis of relaxed configurations, THz analysis; density of states, frontier orbitals, and absorption spectra; coordinates for optimized structures; sample input file for geometry optimizations in SIESTA; and full Gaussian 09 reference. This material is available free of charge via the Internet at http://pubs.acs.org.

■ AUTHOR INFORMATION

Corresponding Authors

*E-mail: robert.crabtree@yale.edu.
*E-mail: charles.schmuttenmaer@yale.edu.
*E-mail: victor.batista@yale.edu.

Notes

The authors declare no competing financial interest.

■ ACKNOWLEDGMENTS

We acknowledge support by the U.S. Department of Energy Grant DE-FG02-07ER15909 (C.A.S) and DE-PS02-08ER15944 (R.H.C). Computational work was supported as part of the Argonne-Northwestern Solar Energy Research (ANSER) Center, an Energy Frontier Research Center funded by the U.S. Department of Energy, Office of Science, Office of Basic Energy Sciences under Award Number DE-SC0001059 (V.S.B). Computer resources were provided by NERSC and by the High performance Computing facilities at Yale University.

■ REFERENCES

(1) O'Regan, B.; Grätzel, M. A Low-Cost, High-Efficiency Solar-Cell Based on Dye-Sensitized Colloidal Tio_2 Films. *Nature* **1991**, *353*, 737−740.

(2) Hagfeldt, A.; Boschloo, G.; Sun, L. C.; Kloo, L.; Pettersson, H. Dye-Sensitized Solar Cells. *Chem. Rev.* **2010**, *110*, 6595−6663.
(3) Beek, W. J. E.; Wienk, M. M.; Janssen, R. A. J. Hybrid Solar Cells from Regioregular Polythiophene and ZnO Nanoparticles. *Adv. Funct. Mater.* **2006**, *16*, 1112−1116.
(4) Kwong, C. Y.; Choy, W. C. H.; Djurisic, A. B.; Chui, P. C.; Cheng, K. W.; Chan, W. K. Poly(3-hexylthiophene): TiO_2 Nanocomposites for Solar Cell Applications. *Nanotechnology* **2004**, *15*, 1156−1161.
(5) Yoshihara, T.; Katoh, R.; Furube, A.; Murai, M.; Tamaki, Y.; Hara, K.; Murata, S.; Arakawa, H.; Tachiya, M. Quantitative Estimation of the Efficiency of Electron Injection from Excited Sensitizer Dye Into Nanocrystalline ZnO Film. *J. Phys. Chem. B* **2004**, *108*, 2643−2647.
(6) Privalov, T.; Boschloo, G.; Hagfeldt, A.; Svensson, P. H.; Kloo, L. A Study of the Interactions between I-/I-3(-) Redox Mediators and Organometallic Sensitizing Dyes in Solar Cells. *J. Phys. Chem. C* **2009**, *113*, 783−790.
(7) Bessho, T.; Yoneda, E.; Yum, J. H.; Guglielmi, M.; Tavernelli, I.; Imai, H.; Rothlisberger, U.; Nazeeruddin, M. K.; Grätzel, M. New Paradigm in Molecular Engineering of Sensitizers for Solar Cell Applications. *J. Am. Chem. Soc.* **2009**, *131*, 5930−5934.
(8) Grätzel, M. Solar Energy Conversion by Dye-Sensitized Photovoltaic Cells. *Inorg. Chem.* **2005**, *44*, 6841−6851.
(9) Grätzel, M. Recent Advances in Sensitized Mesoscopic Solar Cells. *Acc. Chem. Res.* **2009**, *42*, 1788−1798.
(10) Grätzel, M. Photoelectrochemical Cells. *Nature* **2001**, *414*, 338−344.
(11) Mishra, A.; Fischer, M. K. R.; Bauerle, P. Metal-Free Organic Dyes for Dye-Sensitized Solar Cells: From Structure: Property Relationships to Design Rules. *Angew. Chem.-Int. Edit.* **2009**, *48*, 2474−2499.
(12) Qin, P.; Zhu, H. J.; Edvinsson, T.; Boschloo, G.; Hagfeldt, A.; Sun, L. C. Design of an Organic Chromophore For P-Type Dye-Sensitized Solar Cells. *J. Am. Chem. Soc.* **2008**, *130*, 8570−8571.
(13) Chen, K. F.; Hsu, Y. C.; Wu, Q. Y.; Yeh, M. C. P.; Sun, S. S. Structurally Simple Dipolar Organic Dyes Featuring 1,3-Cyclohexadiene Conjugated Unit for Dye-Sensitized Solar Cells. *Org. Lett.* **2009**, *11*, 377−380.
(14) Horiuchi, T.; Miura, H.; Sumioka, K.; Uchida, S. High Efficiency of Dye-Sensitized Solar Cells Based on Metal-Free Indoline Dyes. *J. Am. Chem. Soc.* **2004**, *126*, 12218−12219.
(15) Chen, J. H.; Tsai, C. H.; Wang, S. A.; Lin, Y. Y.; Huang, T. W.; Chiu, S. F.; Wu, C. C.; Wong, K. T. Organic Dyes Containing a Coplanar Indacenodithiophene Bridge for High-Performance Dye-Sensitized Solar Cells. *J. Org. Chem.* **2011**, *76*, 8977−8985.
(16) Hoth, C. N.; Schilinsky, P.; Choulis, S. A.; Brabec, C. J. Printing Highly Efficient Organic Solar Cells. *Nano Lett.* **2008**, *8*, 2806−2813.
(17) Kuang, D.; Walter, P.; Nuesch, F.; Kim, S.; Ko, J.; Comte, P.; Zakeeruddin, S. M.; Nazeeruddin, M. K.; Grätzel, M. Co-Sensitization of Organic Dyes for Efficient Ionic Liquid Electrolyte-Based Dye-Sensitized Solar Cells. *Langmuir* **2007**, *23*, 10906−10909.
(18) Mei, J. G.; Graham, K. R.; Stalder, R.; Reynolds, J. R. Synthesis of Isoindigo-Based Oligothiophenes for Molecular Bulk Heterojunction Solar Cells. *Org. Lett.* **2010**, *12*, 660−663.
(19) Zhang, M.; Wang, Y.; Xu, M.; Ma, W.; Li, R.; Wang, P. Design of High-Efficiency Organic Dyes for Titania Solar Cells Based On The Chromophoric Core of Cyclopentadithiophene-Benzothiadiazole. *Energy Environ. Sci.* **2013**, *6*, 2944−2949.
(20) Yella, A.; Lee, H.-W.; Tsao, H. N.; Yi, C.; Chandiran, A. K.; Nazeeruddin, M. K.; Diau, E. W.-G.; Yeh, C.-Y.; Zakeeruddin, S. M.; Grätzel, M. Porphyrin-Sensitized Solar Cells with Cobalt (II/III)−Based Redox Electrolyte Exceed 12% Efficiency. *Science* **2011**, *334*, 629−634.
(21) Bessho, T.; Zakeeruddin, S. M.; Yeh, C.-Y.; Diau, E. W.-G.; Grätzel, M. Highly Efficient Mesoscopic Dye-Sensitized Solar Cells Based on Donor−Acceptor-Substituted Porphyrins. *Angew. Chem., Int. Ed.* **2010**, *49*, 6646−6649.
(22) Imahori, H.; Umeyama, T.; Ito, S. Large pi-Aromatic Molecules as Potential Sensitizers for Highly Efficient Dye-Sensitized Solar Cells. *Acc. Chem. Res.* **2009**, *42*, 1809−1818.
(23) Lin, C. Y.; Wang, Y. C.; Hsu, S. J.; Lo, C. F.; Diau, E. W. G. Preparation and Spectral, Electrochemical, and Photovoltaic Properties of Acene-Modified Zinc Porphyrins. *J. Phys. Chem. C* **2010**, *114*, 687−693.
(24) Campbell, W. M.; Burrell, A. K.; Officer, D. L.; Jolley, K. W. Porphyrins as Light Harvesters in The Dye-Sensitised Tio_2 Solar Cell. *Coord. Chem. Rev.* **2004**, *248*, 1363−1379.
(25) Martini, L. A.; Moore, G. F.; Milot, R. L.; Cai, L. Z.; Sheehan, S. W.; Schmuttenmaer, C. A.; Brudvig, G. W.; Crabtree, R. H. Modular Assembly of High-Potential Zinc Porphyrin Photosensitizers Attached to TiO_2 with a Series of Anchoring Groups. *J. Phys. Chem. C* **2013**, *117*, 14526−14533.
(26) Brumbach, M. T.; Boal, A. K.; Wheeler, D. R. Metalloporphyrin Assemblies on Pyridine-Functionalized Titanium Dioxide. *Langmuir* **2009**, *25*, 10685−10690.
(27) Subbaiyan, N. K.; Hill, J. P.; Ariga, K.; Fukuzumi, S.; D'Souza, F. Enhanced Photocurrents via Redox Modulation By Fluoride Binding to Oxoporphyrinogen in a Zinc Porphyrin-Oxoporphyrinogen Surface Modified TiO_2 Supramolecular Solar Cell. *Chem. Commun.* **2011**, *47*, 6003−6005.
(28) Subbaiyan, N. K.; Wijesinghe, C. A.; D'Souza, F. Supramolecular Solar Cells: Surface Modification of Nanocrytalline TiO_2 with Coordinating Ligands To Immobilize Sensitizers and Dyads via Metal-Ligand Coordination for Enhanced Photocurrent Generation. *J. Am. Chem. Soc.* **2009**, *131*, 14646−14647.
(29) Moore, G. F.; Konezny, S. J.; Song, H. E.; Milot, R. L.; Blakemore, J. D.; Lee, M. L.; Batista, V. S.; Schmuttenmaer, C. A.; Crabtree, R. H.; Brudvig, G. W. Bioinspired High-Potential Porphyrin Photoanodes. *J. Phys. Chem. C* **2012**, *116*, 4892−4902.
(30) Moore, G. F.; Blakemore, J. D.; Milot, R. L.; Hull, J. F.; Song, H. E.; Cai, L.; Schmuttenmaer, C. A.; Crabtree, R. H.; Brudvig, G. W. A Visible Light Water-Splitting Cell with a Photoanode Formed By Codeposition of a High-Potential Porphyrin and an Iridium Water-Oxidation Catalyst. *Energy Environ. Sci.* **2011**, *4*, 2389−2392.
(31) Stockwell, D.; Yang, Y.; Huang, J.; Anfuso, C.; Huang, Z. Q.; Lian, T. Q. Comparison of Electron-Transfer Dynamics from Coumarin 343 to TiO_2, SnO_2, and ZnO Nanocrystalline Thin Films: Role of Interface-Bound Charge-Separated Pairs. *J. Phys. Chem. C* **2010**, *114*, 6560−6566.
(32) Nazeeruddin, M. K.; De Angelis, F.; Fantacci, S.; Selloni, A.; Viscardi, G.; Liska, P.; Ito, S.; Bessho, T.; Grätzel, M. Combined Experimental and DFT-TDDFT Computational Study of Photoelectrochemical Cell Ruthenium Sensitizers. *J. Am. Chem. Soc.* **2005**, *127*, 16835−16847.
(33) Lin, L. Y.; Tsai, C. H.; Wong, K. T.; Huang, T. W.; Hsieh, L.; Liu, S. H.; Lin, H. W.; Wu, C. C.; Chou, S. H.; Chen, S. H.; et al. Organic Dyes Containing Coplanar Diphenyl-Substituted Dithienosilole Core for Efficient Dye-Sensitized Solar Cells. *J. Org. Chem.* **2010**, *75*, 4778−4785.
(34) Snaith, H. J.; Zakeeruddin, S. M.; Wang, Q.; Pechy, P.; Grätzel, M. Dye-Sensitized Solar Cells Incorporating a "Liquid" Hole-Transporting Material. *Nano Lett.* **2006**, *6*, 2000−2003.
(35) Pensack, R. D.; Asbury, J. B. Beyond the Adiabatic Limit: Charge Photogeneration in Organic Photovoltaic Materials. *J. Phys. Chem. Lett.* **2010**, *1*, 2255−2263.
(36) Xiao, D. Q.; Martini, L. A.; Snoeberger, R. C.; Crabtree, R. H.; Batista, V. S. Inverse Design and Synthesis of acac-Coumarin Anchors for Robust TiO_2 Sensitization. *J. Am. Chem. Soc.* **2011**, *133*, 9014−9022.
(37) De Angelis, F. Direct vs. Indirect Injection Mechanisms in Perylene Dye-Sensitized Solar Cells: A DFT/TDDFT Investigation. *Chem. Phys. Lett.* **2010**, *493*, 323−327.
(38) Tae, E. L.; Lee, S. H.; Lee, J. K.; Yoo, S. S.; Kang, E. J.; Yoon, K. B. A Strategy to Increase the Efficiency of the Dye-Sensitized TiO_2 Solar Cells Operated By Photoexcitation of Dye-to-TiO_2 Charge-Transfer Bands. *J. Phys. Chem. B* **2005**, *109*, 22513−22522.

(39) Koops, S. E.; Barnes, P. R. F.; O'Regan, B. C.; Durrant, J. R. Kinetic Competition in a Coumarin Dye-Sensitized Solar Cell: Injection and Recombination Limitations upon Device Performance. *J. Phys. Chem. C* **2010**, *114*, 8054−8061.
(40) De Angelis, F.; Fantacci, S.; Selloni, A. Alignment Of The Dye's Molecular Levels With The Tio_2 Band Edges In Dye-Sensitized Solar Cells: a DFT-TDDFT Study. *Nanotechnology* **2008**, *19*, 424002.
(41) Duncan, W. R.; Stier, W. M.; Prezhdo, O. V. Ab Initio Nonadiabatic Molecular Dynamics of the Ultrafast Electron Injection Across The Alizarin-TiO_2 Interface. *J. Am. Chem. Soc.* **2005**, *127*, 7941−7951.
(42) Duncan, W. R.; Prezhdo, O. V. Theoretical Studies of Photoinduced Electron Transfer in Dye-Sensitized TiO_2. *Annu. Rev. Phys. Chem.* **2007**, *58*, 143−184.
(43) Oviedo, M. B.; Zarate, X.; Negre, C. F. A.; Schott, E.; Arratia-Perez, R.; Sanchez, C. G. Quantum Dynamical Simulations as a Tool for Predicting Photoinjection Mechanisms in Dye-Sensitized TiO_2 Solar Cells. *J. Phys. Chem. Lett.* **2012**, *3*, 2548−2555.
(44) Ramakrishna, G.; Ghosh, H. N.; Singh, A. K.; Palit, D. K.; Mittal, J. P. Dynamics of Back-Electron Transfer Processes of Strongly Coupled Triphenyl Methane Dyes Adsorbed On TiO_2 Nanoparticle Surface as Studied by Fast and Ultrafast Visible Spectroscopy. *J. Phys. Chem. B* **2001**, *105*, 12786−12796.
(45) Turner, G. M.; Beard, M. C.; Schmuttenmaer, C. A. Carrier Localization And Cooling in Dye-Sensitized Nanocrystalline Titanium Dioxide. *J. Phys. Chem. B* **2002**, *106*, 11716−11719.
(46) Wang, Y. H.; Hang, K.; Anderson, N. A.; Lian, T. Q. Comparison of Electron Transfer Dynamics in Molecule-to-Nanoparticle and Intramolecular Charge Transfer Complexes. *J. Phys. Chem. B* **2003**, *107*, 9434−9440.
(47) Anderson, N. A.; Lian, T. Q. Ultrafast Electron Transfer at the Molecule-Semiconductor Nanoparticle Interface. *Annu. Rev. Phys. Chem.* **2005**, *56*, 491−519.
(48) Furube, A.; Katoh, R.; Hara, K.; Sato, T.; Murata, S.; Arakawa, H.; Tachiya, M. Lithium Ion Effect on Electron Injection from a Photoexcited Coumarin Derivative into a TiO_2 Nanocrystalline Film Investigated by Visible-to-IR Ultrafast Spectroscopy. *J. Phys. Chem. B* **2005**, *109*, 16406−16414.
(49) McNamara, W. R.; Snoeberger, R. C.; Li, G.; Schleicher, J. M.; Cady, C. W.; Poyatos, M.; Schmuttenmaer, C. A.; Crabtree, R. H.; Brudvig, G. W.; Batista, V. S. Acetylacetonate Anchors for Robust Functionalization of TiO_2 Nanoparticles with Mn(II)-Terpyridine Complexes. *J. Am. Chem. Soc.* **2008**, *130*, 14329−14338.
(50) McNamara, W. R.; Snoeberger, R. C.; Li, G. H.; Richter, C.; Allen, L. J.; Milot, R. L.; Schmuttenmaer, C. A.; Crabtree, R. H.; Brudvig, G. W.; Batista, V. S. Hydroxamate Anchors for Water-Stable Attachment to TiO_2 Nanoparticles. *Energ. Environ. Sci.* **2009**, *2*, 1173−1175.
(51) Rego, L. G. C.; Batista, V. S. Quantum Dynamics Simulations of Interfacial Electron Transfer in Sensitized TiO_2 Semiconductors. *J. Am. Chem. Soc.* **2003**, *125*, 7989−7997.
(52) Duncan, W. R.; Prezhdo, O. V. Nonadiabatic Molecular Dynamics Study of Electron Transfer from Alizarin to the Hydrated Ti^{4+} ion. *J. Phys. Chem. B* **2005**, *109*, 17998−18002.
(53) Duncan, W. R.; Prezhdo, O. V. Temperature Independence Of the Photoinduced Electron Injection in Dye-Sensitized TiO_2 Rationalized by Ab Initio Time-Domain Density Functional Theory. *J. Am. Chem. Soc.* **2008**, *130*, 9756−9762.
(54) Sanchez-de-Armas, R.; Lopez, J. O.; San-Miguel, M. A.; Sanz, J. F.; Ordejon, P.; Pruneda, M. Real-Time TD-DFT Simulations in Dye Sensitized Solar Cells: The Electronic Absorption Spectrum of Alizarin Supported on TiO_2 Nanoclusters. *J. Chem. Theory Comput.* **2010**, *6*, 2856−2865.
(55) Li, J. R.; Kondov, I.; Wang, H. B.; Thoss, M. Theoretical Study of Photoinduced Electron-Transfer Processes in the Dye- Semiconductor System Alizarin-TiO_2. *J. Phys. Chem. C* **2010**, *114*, 18481−18493.
(56) Rocca, D.; Gebauer, R.; De Angelis, F.; Nazeeruddin, M. K.; Baroni, S. Time-Dependent Density Functional Theory Study Of Squaraine Dye-Sensitized Solar Cells. *Chem. Phys. Lett.* **2009**, *475*, 49−53.
(57) Jakubikova, E.; Snoeberger, R. C.; Batista, V. S.; Martin, R. L.; Batista, E. R. Interfacial Electron Transfer in TiO_2 Surfaces Sensitized with Ru(II)-Polypyridine Complexes. *J. Phys. Chem. A* **2009**, *113*, 12532−12540.
(58) Kusama, H.; Sugihara, H.; Sayama, K. Nitrogen-Containing Heterocycles' Interaction with Ru Dye in Dye-Sensitized Solar Cells. *J. Phys. Chem. C* **2009**, *113*, 20764−20771.
(59) Odom, S. A.; Kelley, R. F.; Ohira, S.; Ensley, T. R.; Huang, C.; Padilha, L. A.; Webster, S.; Coropceanu, V.; Barlow, S.; Hagan, D. J.; et al. Photophysical Properties of an Alkyne-Bridged Bis(zinc porphyrin)-Perylene Bis(dicarboximide) Derivative. *J. Phys. Chem. A* **2009**, *113*, 10826−10832.
(60) Ernstorfer, R.; Gundlach, L.; Felber, S.; Storck, W.; Eichberger, R.; Willig, F. Role of Molecular Anchor Groups In Molecule-To-Semiconductor Electron Transfer. *J. Phys. Chem. B* **2006**, *110*, 25383−25391.
(61) Nilsing, M.; Persson, P.; Ojamae, L. Anchor Group Influence on Molecule-Metal Oxide Interfaces: Periodic Hybrid DFT Study of Pyridine Bound to TiO_2 via Carboxylic and Phosphonic Acid. *Chem. Phys. Lett.* **2005**, *415*, 375−380.
(62) She, C. X.; Guo, J. C.; Irle, S.; Morokuma, K.; Mohler, D. L.; Zabri, H.; Odobel, F.; Youm, K. T.; Liu, F.; Hupp, J. T.; et al. Comparison of Interfacial Electron Transfer Through Carboxylate And Phosphonate Anchoring Groups. *J. Phys. Chem. A* **2007**, *111*, 6832−6842.
(63) McNamara, W. R.; Milot, R. L.; Song, H. E.; Snoeberger, R. C.; Batista, V. S.; Schmuttenmaer, C. A.; Brudvig, G. W.; Crabtree, R. H. Water-Stable, Hydroxamate Anchors for Functionalization of Tio_2 Surfaces with Ultrafast Interfacial Electron Transfer. *Energy Environ. Sci.* **2010**, *3*, 917−923.
(64) Hirao, T.; Masunaga, T.; Ohshiro, Y.; Agawa, T. A Novel Synthesis of Dialkyl Arenephosphonates. *Synth.-Stuttgart.* **1981**, *1*, 56−57.
(65) Konar, S.; Zoń, J.; Prosvirin, A. V.; Dunbar, K. R.; Clearfield, A. Synthesis and Characterization of Four Metal−Organophosphonates with One-, Two-, and Three-Dimensional Structures. *In. Chem.* **2007**, *46*, 5229−5236.
(66) Mackay, L. G.; Anderson, H. L.; Sanders, J. K. M. A Platinum-Linked Porphyrin Trimer and a Complementary Aluminium tris[3-(4-pyridyl)acetylacetonate] Guest. *J. Chem. Soc.-Perkin Trans.* **1995**, *1*, 2269−2273.
(67) Mulcahy, C.; Krot, K. A.; Griffith, D. M.; Suponitsky, K. Y.; Starikova, Z. A.; Marmion, C. J. Iron(III) Tris(pyridinehydroxamate)s and Related Nickel(II) and Zinc(II) Complexes: Potential Platforms for the Design of Novel Heterodimetallic Supramolecular Assemblies. *Eur. J. Inorg. Chem.* **2007**, *10*, 1373−1380.
(68) Spampinato, V.; Tuccitto, N.; Quici, S.; Calabrese, V.; Marletta, G.; Torrisi, A.; Licciardello, A. Functionalization of Oxide Surfaces by Terpyridine Phosphonate Ligands: Surface Reactions and Anchoring Geometry. *Langmuir* **2010**, *26*, 8400−8406.
(69) Beard, M. C.; Turner, G. M.; Schmuttenmaer, C. A. Transient Photoconductivity in GaAs as Measured by Time-Resolved Terahertz Spectroscopy. *Phys. Rev. B* **2000**, *62*, 15764−15777.
(70) Beard, M. C.; Turner, G. M.; Schmuttenmaer, C. A. Subpicosecond Carrier Dynamics in Low-Temperature Grown GaAs as Measured by Time-Resolved Terahertz Spectroscopy. *J. Appl. Phys.* **2001**, *90*, 5915−5923.
(71) Baxter, J. B.; Schmuttenmaer, C. A. Conductivity of ZnO Nanowires, Nanoparticles, and Thin Films Using Time-Resolved Terahertz Spectroscopy. *J. Phys. Chem. B* **2006**, *110*, 25229−25239.
(72) Landauer, R. Electrical Resistance of Disordered One-Dimensional Lattices. *Philos. Mag.* **1970**, *21*, 863−872.
(73) Buttiker, M. 4-Terminal Phase-Coherent Conductance. *Phys. Rev. Lett.* **1986**, *57*, 1761−1764.
(74) Fisher, D. S.; Lee, P. A. Relation Between Conductivity and Transmission Matrix. *Phys. Rev. B* **1981**, *23*, 6851−6854.

(75) Xue, Y. Q.; Datta, S.; Ratner, M. A. First-Principles Based Matrix Green's Function Approach To Molecular Electronic Devices: General Formalism. *Chem. Phys.* **2002**, *281*, 151−170.
(76) Andrews, D. Q.; Cohen, R.; Van Duyne, R. P.; Ratner, M. A. Single Molecule Electron Transport Junctions: Charging and Geometric Effects on Conductance. *J. Chem. Phys.* **2006**, *125*, 174718.
(77) Negre, C. F. A.; Jara, G. E.; Vera, D. M. A.; Pierini, A. B.; Sanchez, C. G. Detailed Analysis of Water Structure in a Solvent Mediated Electron Tunneling Mechanism. *J. Phys.: Condens. Matter* **2011**, *23*, 245305.
(78) Paz, S. A.; Zoloff, M. M. E.; Negre, C. F. A.; Olmos-Asar, J. A.; Mariscal, M. M.; Sánchez, C. G.; Leiva, E. P. M. Configurational Behavior and Conductance of Alkanedithiol Molecular Wires from Accelerated Dynamics Simulations. *J. Chem. Theory Comput.* **2012**, *8*, 4539−4545.
(79) Todorov, T. N.; Briggs, G. A. D.; Sutton, A. P. Elastic Quantum Transport Through Small Structures. *J. Phys.: Condens. Matter* **1993**, *5*, 2389−2406.
(80) Frisch, M. J.; et al. *Gaussian 09*, revision *A.1*; Gaussian, Inc.: Wallingford, CT, 2009.
(81) Yale, H. L. The Hydroxamic Acids. *Chem. Rev.* **1943**, *33*, 209−256.
(82) Morandeira, A.; López-Duarte, I.; Martínez-Díaz, M. V.; O'Regan, B.; Shuttle, C.; Haji-Zainulabidin, N. A.; Torres, T.; Palomares, E.; Durrant, J. R. Slow Electron Injection On Ru−Phthalocyanine Sensitized TiO_2. *J. Am. Chem. Soc.* **2007**, *129*, 9250−9251.
(83) Richter, C.; Schmuttenmaer, C. A. Exciton-Like Trap States Limit Electron Mobility in TiO_2 Nanotubes. *Nat. Nanotechnol.* **2010**, *5*, 769−772.
(84) Brauer, J. C.; Moser, J.-E. Transient Photoconductivity of Dye-Sensitized TiO_2 Nanocrystalline Films Probed by Optical Pump-THz Probe Spectroscopy. In *17th International Conference on Ultrafast Phenomena*; Chergui, M., Jonas, D. M., Riedle, E., Schoenlein, R. W., Taylor, A. J., Eds.; Oxford University Press: New York, 2011; pp 358−360.
(85) Vittadini, A.; Selloni, A.; Rotzinger, F. P.; Grätzel, M. Formic Acid Adsorption on Dry and Hydrated TiO_2 Anatase (101) Surfaces by DFT Calculations. *J. Phys. Chem. B* **2000**, *104*, 1300−1306.
(86) Ambrosio, F.; Martsinovich, N.; Troisi, A. What Is the Best Anchoring Group for a Dye in a Dye-Sensitized Solar Cell? *J. Phys. Chem. Lett.* **2012**, *3*, 1531−1535.
(87) Raghunath, P.; Lin, M. C. Adsorption Configurations and Reactions of Boric Acid on a TiO_2 Anatase (101) Surface. *J. Phys. Chem. C* **2008**, *112*, 8276−8287.
(88) Snoeberger, R. C.; Young, K. J.; Tang, J.; Allen, L. J.; Crabtree, R. H.; Brudvig, G. W.; Coppens, P.; Batista, V. S.; Benedict, J. B. Interfacial Electron Transfer into Functionalized Crystalline Polyoxotitanate Nanoclusters. *J. Am. Chem. Soc.* **2012**, *134*, 8911−8917.
(89) Oviedo, M. B.; Sanchez, C. G. Transition Dipole Moments of the Q(y) Band in Photosynthetic Pigments. *J. Phys. Chem. A* **2011**, *115*, 12280−12285.
(90) Koyama, Y.; Kakitani, Y.; Nagae, H. Mechanisms of Suppression and Enhancement of Photocurrent/Conversion Efficiency in Dye-Sensitized Solar-Cells Using Carotenoid and Chlorophyll Derivatives as Sensitizers. *Molecules* **2012**, *17*, 2188−2218.

■ NOTE ADDED AFTER ASAP PUBLICATION

This paper was published ASAP on November 8, 2013, with an error to the affiliations and reference errors to Sections 2 and 3. The corrected version was reposted November 11, 2013.

Supporting Information for:

Efficiency of Interfacial Electron Transfer from Zn-Porphyrin Dyes into TiO_2 Correlated to the Linker Single Molecule Conductance

Christian F. A. Negre, Rebecca L. Milot, Lauren A. Martini, Wendu Ding, Robert H. Crabtree,* Charles A. Schmuttenmaer,* and Victor S. Batista*

Department of Chemistry, Yale University, 225 Prospect St., P.O. Box 208107, New Haven, CT 06520-8107, USA

*E-mail: robert.crabtree@yale.edu, charles.schmuttenmaer@yale.edu, victor.batista@yale.edu

Contents

1.Derivation of Equation 6 **S2**

2. Additional Figures **S4**

3. Optimized Structures **S8**

4. Sample input file for geometry optimizations in SIESTA **S38**

5. Full Gaussian09 Reference **S41**

Derivation of B(t) Formula

As shown in Figure 6a of the main text, we consider the injection of an electron from the semiconductor surface (X) to the TiO_2 conduction band (B).

$$X \xrightarrow{k_1} B \tag{S1}$$

where k_1 is the injection rate constant. In addition, the injected carriers can equilibrate with trap states C,

$$B \underset{k_3}{\overset{k_2}{\longleftrightarrow}} C \tag{S2}$$

where the rate constant for trapping is k_2 and that for detrapping is k_3. From this, the following kinetic model is obtained:

$$\begin{aligned} \frac{dX}{dt} &= -k_1 X, \\ \frac{dB}{dt} &= +k_1 X - k_2 B + k_3 C, \\ \frac{dC}{dt} &= +k_2 B - k_3 C, \\ X_0 &= X + B + C\ . \end{aligned} \tag{S3}$$

Solving for X from the first line of Eq. S3 yields $X = X_0 e^{-k_1 t}$, and solving for C, we obtain:

$$\begin{aligned} C &= X_0 - X - B, \\ C &= X_0 - X_0 e^{-k_1 t} - B. \end{aligned} \tag{S4}$$

Inserting the last line of Eq. S4 into the second line of Eq. S3, we obtain:

$$\frac{dB}{dt} = k_1 X_0 e^{-k_1 t} - k_2 B + k_3 X_0 - k_3 X_0 e^{-k_1 t} - k_3 B, \tag{S5}$$

or

$$\frac{dB}{dt} = -(k_2 + k_3) B + k_3 X_0 + X_0 e^{-k_1 t} (k_1 - k_3), \tag{S6}$$

Solving for $B(t)$ we obtain:

$$B(t) = \frac{k_3 X_0}{k_2 + k_3} + \frac{X_0(k_1 - k_3)}{-k_1 + k_2 + k_3} e^{-k_1 t} + \theta_3 e^{-(k_2 + k_3)t} \tag{S7}$$

letting $t = 0$, we find that:

$$\theta_3 = \frac{X_0 k_1 k_2}{(k_2 + k_3)(k_1 - k_2 - k_3)} \tag{S8}$$

We let $\theta_1 = \frac{k_3 X_0}{k_2 + k_3}$ and $\theta_2 = \frac{X_0(k_1 - k_3)}{-k_1 + k_2 + k_3}$ and substitution into Equation S7 yields

$$B(t) = X_0\left(\theta_1 + \theta_2 e^{-k_1 t} + \theta_3 e^{-(k_2 + k_3)t}\right) \tag{S9}$$

When $k_3 \to 0$, we recover the familiar solution for consecutive elementary processes $X \xrightarrow{k_1} B \xrightarrow{k_2} C$:

$$B(t) = -\frac{k_1 E_0\left(e^{-k_1 t} - e^{-k_2 t}\right)}{k_2 - k_1} \tag{S10}$$

When $k_3 \to 0$ and $k_2 \to 0$ we are left with the solution for $E \xrightarrow{k_1} B$:

$$B(t) = E_0(1 - e^{-k_1 t}) \tag{S11}$$

Values for X_0, k_1, k_2, and k_3 were obtained by performing a nonlinear least squares fit of Equation S9 (Equation 6 in the main text) to the measured transient THz absorption data and are given in Table 2. A global fit was performed wherein k_2 and k_3 were varied simultaneously for all linkers, but each linker had its own independent values of X_0 and k_1.

Table S1: Fitting parameters for B(t) function. $k_2 = 0.386$ ps^{-1} and and $k_3 = 0.253$ ps^{-1}.

Linker	X_0 **(Arb. Units)**	k_1 **(ps^{-1})**	τ_1 **(ps)**
L1	6.95	0.70	1.42
L2	4.56	0.58	1.73
L3	3.76	0.83	1.20
L4	9.31	0.70	1.42
L5	4.29	0.65	1.54

Additional figures

The principal electronic transition frequencies and oscillator strengths for L-$ZnPF_{10}$ dyes were calculated at the TDDFT (B3LYP/LANL2DZ) level of theory. The general spectral features shown in Figure S1 agree with the experimental UV-vis data, as shown in Figure 4 of the main text. From Figure S1, we see that free $ZnPF_{10}$-diester absorbs at a slightly shorter wavelength than the linker-porphyrin complexes (L-$ZnPF_{10}$). The red-shift in the porphyrin absorption spectrum upon axial coordination of pyridyl ligands is also observed in the experimental UV-vis and is well-established in the literature. The magnitude of the red-shift was the same for all the linkers (L1-L5) considered in this work. Additionally, we found that L5-$ZnPF_{10}$ and L3-$ZnPF_{10}$ have calculated absorptivities at 400 nm that are about 30% larger than for the other complexes. Also, the absorption intensity of L4-$ZnPF_{10}$ is similar to that of L1-$ZnPF_{10}$. These observations reinforce that the trends in electron injection efficiency determined by THz spectroscopy (Figure 5 of the main text) cannot be explained by considering experiemntal or calculated absorption intensities alone.

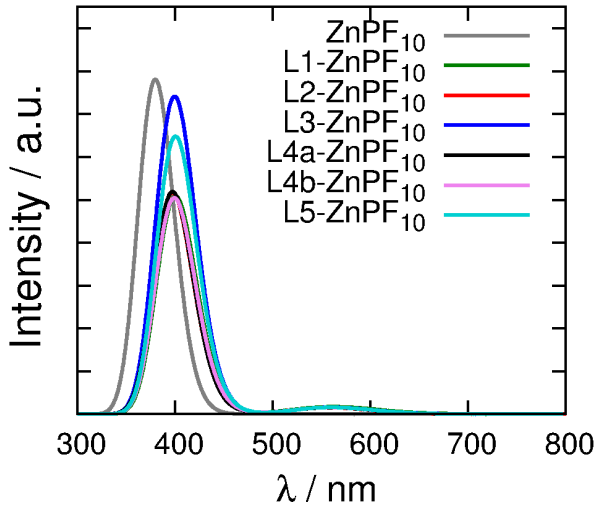

Figure S1: Absorption spectra for L-$ZnPF_{10}$ complexes. The computed absorption bands have been convoluted with Gaussian functions with a FWHM of 0.4 eV to model the inhomogeneous broadening.

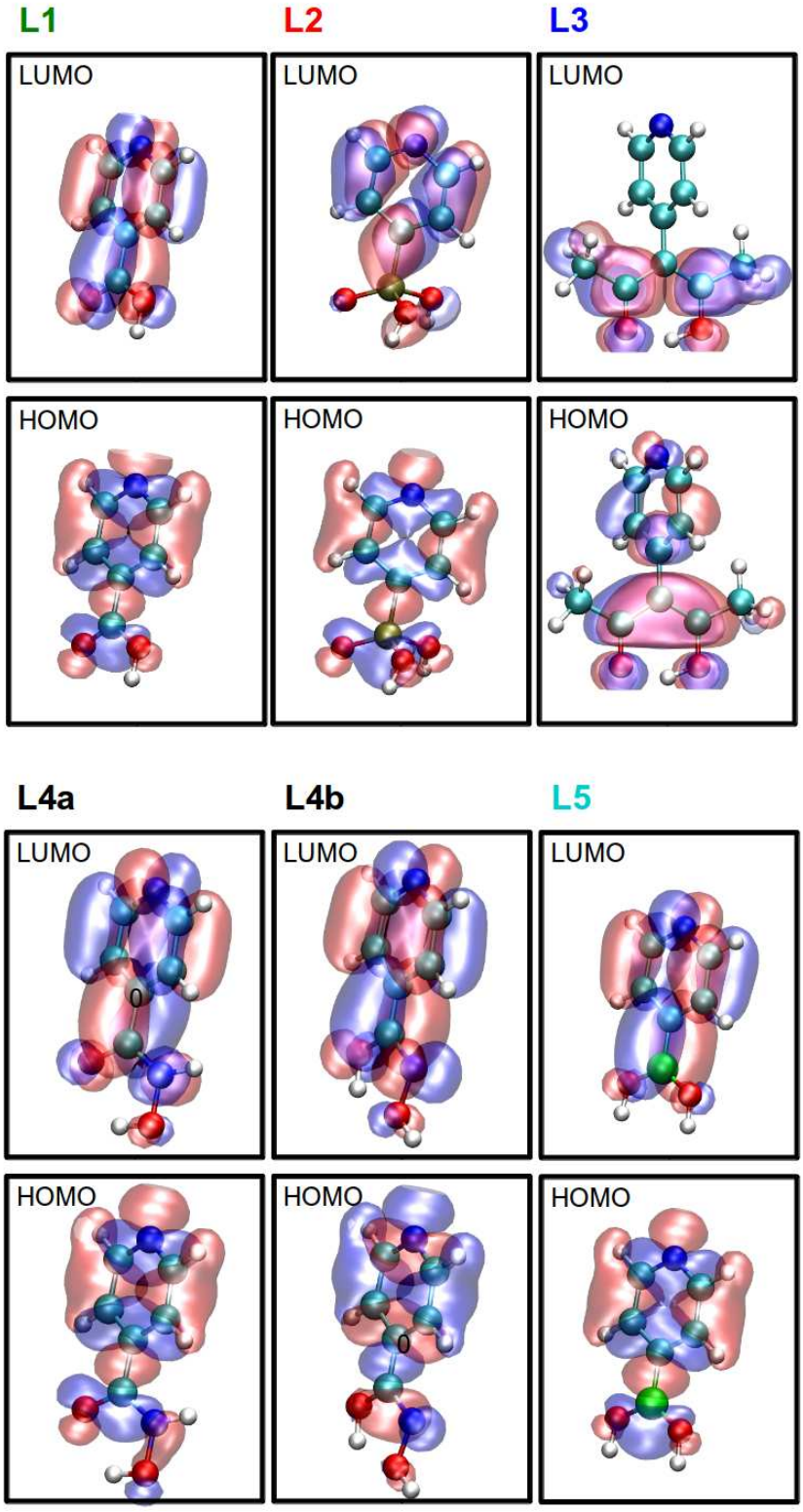

Figure S2: Frontier orbitals calculated within the extended Hückel Hamiltonian for all the linkers considered here.

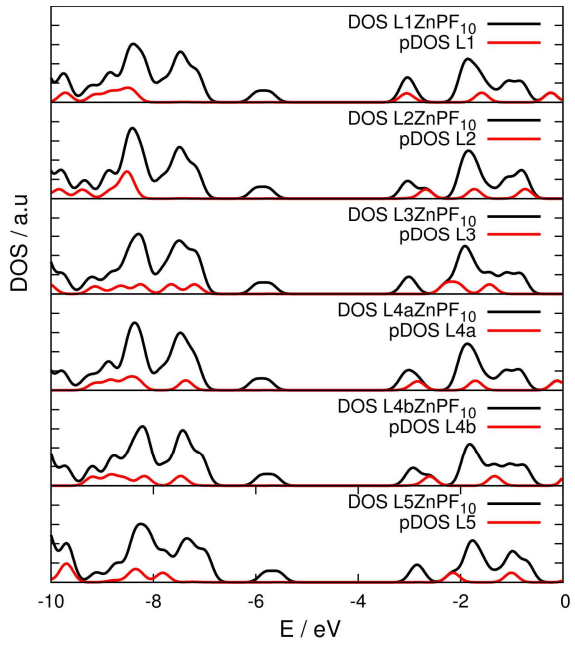

Figure S3: DOS for all the L-ZnPF10 (black line), and DOS projected onto the linkers (pDOS) (red lines). For all the cases the Fermi level of L-ZnPF10 is around -4.44 eV.

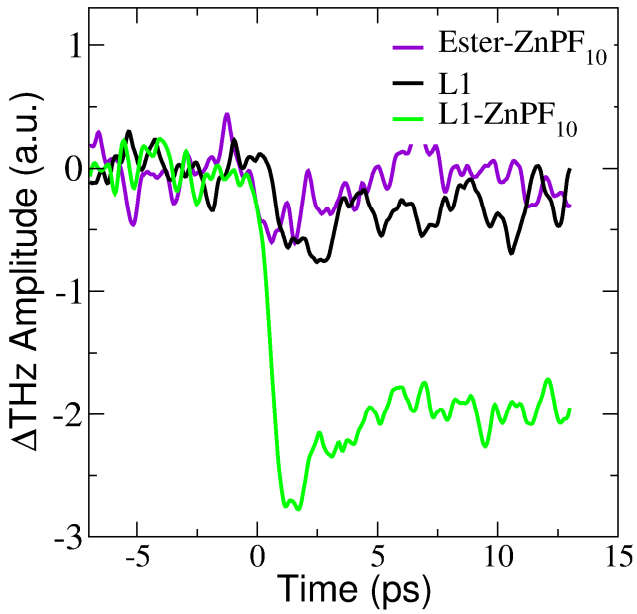

Figure S4: Comparison of sensitization with L1(only linker) and L1-$ZnPF_{10}$. The figure shows a big difference in e-injection. The case of just the ligand L1 resembles the Ester-$ZnPF_{10}$ where hardly any injection is observed.

Geometry optimization for sensitized anatase (101) slab has been performed at the DFT/GGA level of theory by using the SIESTA code with periodic boundary conditions. We used a double zeta (DZ) basis set for all atoms. A confinement radius corresponding to an energy shift of 0.01 eV was employed. A 200 Ry kinetic energy grid cut-off was used. Optimization was done with a force tolerance of 0.04 eV Å−1 fixing the lower layer of Ti atoms and relaxing the rest of the structure. Only the Γ point was used in reciprocal space. Results for L1, L2 and L5 are shown in Figure S4. In all the cases the monodentate mode has a larger binding energy.

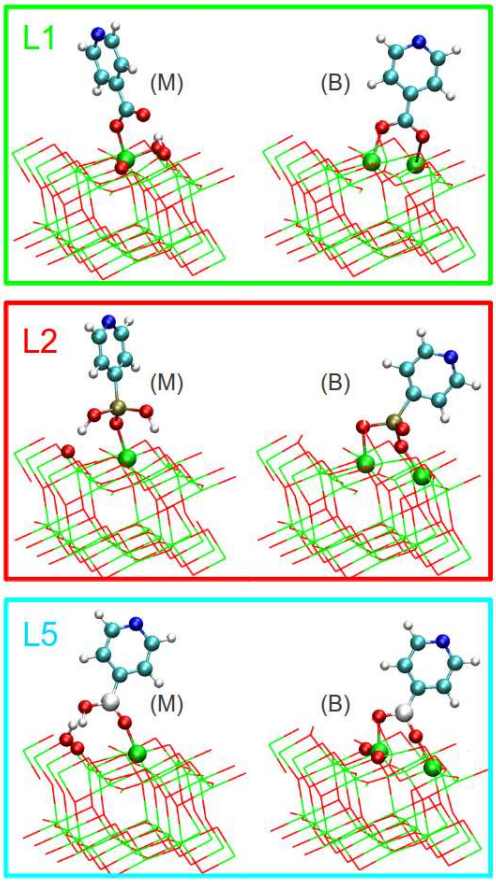

Figure S5: Comparison of relaxed configurations of model nanostructures of TiO2-anatase sensitized with: L1, L2 and L5 anchored to the (101) surface in a monodentate (M) and a chelate-bitentate (B) mode; The binding energies for L1-M, L1-B, L2-M, L5-M and L5-B are 24, 14, 50, 34 and 23 kcal/mol, respectively. L2-B is predicted to be unstable. Green represents Ti4+ ions, red represents O2- ions, light blue represents C atoms, deep blue represents N, light brown represents P, large white spheres represent B, and small gray spheres represent H atoms.

Optimized Structures

All optimization were performed using Gaussian09.C01 program, with B3LYP/LANL2DZ level for all atoms.

Table S3-1. Atomic coordinates of L1.

C	1.45847900	-1.71455900	0.00000000
N	0.40740700	-2.57605200	0.00000000
C	-0.84475300	-2.05011400	0.00000000
C	-1.09925100	-0.66626600	0.00000000
C	0.00000000	0.21635400	0.00000000
C	1.30541500	-0.31716900	0.00000000
C	-0.17066000	1.69557900	0.00000000
O	-1.50345600	2.08116300	0.00000000
O	0.75320700	2.52637800	0.00000000
H	-1.58079000	3.06205500	0.00000000
H	2.44556200	-2.16831000	0.00000000
H	-1.66148500	-2.76664500	0.00000000
H	-2.11331800	-0.28349500	0.00000000
H	2.16480400	0.34549400	0.00000000

Table S3-2. Atomic coordinates of L2.

C	-2.50890600	1.15681800	-0.00000400
N	-3.17949900	-0.02159700	-0.00000500
C	-2.45319400	-1.16904600	-0.00000400
C	-1.04552100	-1.19088000	-0.00000200
C	-0.37092400	0.04208300	-0.00000100
C	-1.10213200	1.24191700	-0.00000200
P	1.46353900	0.13719600	0.00000200
O	1.86491700	-0.85227600	-1.33749100
O	2.14706200	1.56952500	-0.00000200
H	-3.11938200	2.05548700	-0.00000500
H	-3.02254500	-2.09419200	-0.00000500
H	-0.50859800	-2.13336800	-0.00000200
H	-0.60266200	2.20626900	-0.00000100
O	1.86491500	-0.85226600	1.33750300
H	2.71274800	-0.67307600	1.79395700
H	2.71275500	-0.67309700	-1.79393900

Table S3-3. Atomic coordinates of L3.

C	0.80015200	2.57584800	-0.30636700
H	0.32408300	2.87714600	0.63584500
H	0.00431800	2.49369700	-1.05540900

H	1.51432300	3.34837700	-0.60166200
C	1.54104700	1.26622200	-0.13586700
C	-2.82546000	0.43873500	1.05800100
N	-3.52712600	-0.04435500	0.00030000
C	-2.81363700	-0.51737100	-1.05364700
C	-1.40673300	-0.52296700	-1.09321800
C	-0.67369600	-0.02146800	0.00684600
C	-1.41937200	0.46813800	1.10367900
C	0.82261400	0.00004000	0.00717300
H	-3.41698600	0.80714400	1.89236400
H	-3.39544900	-0.89842300	-1.88915300
H	-0.89029000	-0.90560100	-1.96937400
H	-0.91555400	0.85242400	1.98647000
C	1.56546400	-1.17943500	0.13023600
O	2.92034300	-1.16149800	0.12372000
C	1.00448200	-2.56467900	0.29274500
H	1.25002400	-3.16871400	-0.59056700
H	-0.07737100	-2.56298300	0.43227900
H	1.48438800	-3.04609900	1.15308000
O	2.83008100	1.29117500	-0.13299000
H	3.23583700	-0.18229800	0.02070100

Table S3-4. Atomic coordinates of L4a.

C	2.46807300	1.00999800	-0.16391800
N	3.04891000	-0.21309800	-0.05102300
C	2.23299900	-1.28481000	0.11523000
C	0.83046200	-1.18575400	0.16546200
C	0.23577000	0.08756300	0.03251500
C	1.07661200	1.20756400	-0.12438500
C	-1.24088300	0.31906300	0.07240100
N	-2.05928900	-0.75157900	-0.15731700
O	-1.76986600	1.44973000	0.30736800
O	-3.47189500	-0.53140100	-0.15127100
H	3.14664100	1.84927800	-0.28782400
H	2.72599200	-2.24775000	0.21793700
H	0.24258500	-2.08348000	0.33673400
H	0.64275300	2.19848300	-0.20644400
H	-3.54350600	0.43747200	0.07181700
H	-1.82592800	-1.66964300	-0.50644200

Table S3-5. Atomic coordinates of L4b.

C	-2.45212900	1.00599000	-0.00015700
N	-3.05135900	-0.21165300	-0.00016400
C	-2.24543000	-1.30759400	-0.00003200
C	-0.84343500	-1.23596800	0.00010800

C	-0.23153300	0.03755700	0.00011000
C	-1.05605800	1.18161200	-0.00002400
C	1.23702800	0.18097000	0.00025400
N	2.01695600	-0.87478000	0.00039800
O	1.71321300	1.47377500	0.00031400
O	3.40566700	-0.39545200	-0.00048500
H	-3.11844700	1.86453000	-0.00026300
H	-2.75196100	-2.26901400	-0.00004100
H	-0.23971900	-2.13704300	0.00021200
H	-0.61794200	2.17310600	-0.00002400
H	3.94301900	-1.21278700	-0.00036700
H	2.69911900	1.46507900	0.00045800

Table S3-6. Atomic coordinates of L5.

C	-1.97256800	1.16120400	-0.00015400
N	-2.67818700	0.00000200	0.00000000
C	-1.97256300	-1.16120700	0.00015400
C	-0.56630000	-1.20690800	0.00015100
C	0.17330300	0.00000300	0.00000100
C	-0.56629900	1.20690600	-0.00015000
B	1.73122800	-0.00000900	0.00000500
O	2.37843800	-1.22569300	-0.00030000
H	-2.56308700	2.07422300	-0.00028000
H	-2.56308700	-2.07422000	0.00028000
H	-0.05096000	-2.16262500	0.00025000
H	-0.05096100	2.16262200	-0.00024900
O	2.37843100	1.22568000	0.00029600
H	3.34542100	1.32642400	0.00027600
H	3.34545400	-1.32628100	-0.00026800

Table S3-7. Atomic coordinates of L1ZnPF$_{10}$.

N	-0.05977600	0.02820800	1.99838100
C	-0.29865100	-1.11818600	2.69022700
C	-0.35009700	-1.14924200	4.09143100
C	-0.14998400	0.05105200	4.80240900
C	0.09615500	1.23994900	4.08791800
C	0.13449900	1.18455500	2.68591900
C	-0.20700900	0.01921700	6.29346200
O	-0.42586200	-0.99290100	6.97716800
O	0.01369400	1.26368500	6.85843900
H	-0.02837300	1.21947000	7.84053400
H	0.25250700	2.17689900	4.60868300
H	0.32410200	2.07482200	2.09717700
H	-0.45095000	-2.01726900	2.10405000
H	-0.53965700	-2.07587700	4.62236000

C	2.84186700	-1.29963100	-0.52505400
N	1.46261100	-1.48006800	-0.52845300
C	1.22946300	-2.84829400	-0.51795800
C	2.50505000	-3.55805500	-0.48276700
C	3.49589000	-2.60702400	-0.48730200
C	-0.04407300	-3.46201600	-0.54614800
C	-1.29285700	-2.80197400	-0.62084900
C	-2.58371800	-3.46310400	-0.78640300
C	-3.53699800	-2.47586300	-0.85169500
C	-2.84524900	-1.19545400	-0.71368100
N	-1.48040100	-1.42774000	-0.57655800
C	-3.47503000	0.07431600	-0.75209300
C	-2.79927700	1.32022900	-0.71159300
C	-3.45365700	2.62780500	-0.72960100
C	-2.46440500	3.57905400	-0.67588600
C	-1.18946100	2.86913500	-0.62389300
N	-1.42225700	1.50092400	-0.63264600
C	0.08367100	3.48276100	-0.57995500
C	1.33457100	2.82274200	-0.57089500
C	2.63335500	3.48264000	-0.66328400
C	3.58850400	2.49501700	-0.66080200
C	2.88921800	1.21577800	-0.55265800
N	1.51866600	1.44901100	-0.50173900
C	3.51954700	-0.05421500	-0.53970400
H	4.56253900	-2.77207700	-0.45946400
C	-0.07899800	-4.96081100	-0.48825800
H	-2.74248800	-4.52885400	-0.87230800
H	-4.59917600	-2.59927400	-1.00188600
C	-4.97306900	0.09948700	-0.86472500
H	-4.51984600	2.79309200	-0.76992400
H	-2.59280800	4.65224700	-0.67553500
C	0.11497800	4.98211500	-0.53449300
H	2.79760900	4.54755900	-0.74936800
H	4.65794500	2.61750100	-0.74636500
C	5.02152700	-0.08062200	-0.56443700
H	2.63297200	-4.63105000	-0.46047600
Zn	0.00957000	0.01240100	-0.23661800
C	-0.37025000	-5.63207400	0.71179600
C	-0.41463900	-7.02780100	0.80666300
C	-0.15947100	-7.80125400	-0.33217400
C	0.13533400	-7.17051500	-1.54659600
C	0.17151100	-5.77104500	-1.60861900
F	-0.61692500	-4.89315300	1.86129400
F	-0.70333600	-7.64402400	2.00820900
F	-0.19888200	-9.17742600	-0.25719200
F	0.38503900	-7.93004100	-2.67221100
F	0.45751500	-5.18145000	-2.82767400
C	0.32066900	5.66507100	0.67654800

C	0.35782100	7.06161000	0.76103200
C	0.18391400	7.82408400	-0.40027700
C	-0.02397100	7.18154800	-1.62645100
C	-0.05576900	5.78143700	-1.67741900
F	0.56016300	7.68933900	1.97444400
F	0.48624600	4.93751300	1.84802000
F	0.21746900	9.20091400	-0.33550100
F	-0.19349200	7.93000000	-2.77407100
F	-0.25521200	5.18005000	-2.90768700
C	5.71629700	-0.60337400	-1.68060600
C	7.11904300	-0.62467600	-1.71070000
C	7.85624500	-0.12794300	-0.61394900
C	7.17279700	0.39344400	0.50611000
C	5.77103000	0.42024900	0.52622400
C	-5.78350400	-0.38720800	0.18770800
C	-7.18319300	-0.36244000	0.09061600
C	-7.80062200	0.14396800	-1.07344500
C	-7.00106800	0.62609500	-2.13271500
C	-5.60308000	0.60738600	-2.02569600
H	5.24985100	0.81505300	1.39417000
H	7.75202900	0.76851200	1.34492700
C	9.34442300	-0.13288000	-0.59454200
H	7.64782700	-1.01801300	-2.57216900
H	5.15226100	-0.97651200	-2.53112300
H	-4.99253100	0.97006400	-2.84811700
H	-7.48844800	1.00660800	-3.02570200
C	-9.28020600	0.18826000	-1.22768100
H	-7.80122800	-0.72786900	0.90362400
H	-5.31184500	-0.77054400	1.08858500
O	10.04916000	0.29392700	0.34062400
O	9.88937300	-0.67216000	-1.74605300
C	11.35986100	-0.72026100	-1.82345700
H	11.57567900	-1.17647600	-2.79054500
H	11.77406800	0.29108100	-1.76318200
O	-9.88253000	0.62345700	-2.22802900
O	-9.94575400	-0.31382300	-0.12308000
C	-11.41795700	-0.31191600	-0.18101200
H	-11.73749700	-0.73542700	0.77216300
H	-11.78947200	0.71032300	-0.30333000
H	11.76120900	-1.32417600	-1.00360400
H	-11.76303100	-0.92389000	-1.02030100

Table S3-8. Atomic coordinates of L2ZnPF$_{10}$.

N	-0.05946600	0.01755600	1.77307100
C	-0.10838400	-1.16355900	2.44459000
C	-0.16260800	-1.22861800	3.84594900
C	-0.16392800	-0.02135300	4.56488200

C	-0.11857100	1.20461800	3.88062500
C	-0.06531500	1.17891200	2.47610400
P	-0.22707600	-0.00331500	6.40795800
O	-1.42416600	-1.17908200	6.66769900
O	1.14332900	-0.88990800	6.95053100
H	-0.13094200	2.14982800	4.41452300
H	-0.02912600	2.09875000	1.90342200
H	-0.10528400	-2.06671600	1.84487700
H	-0.21124100	-2.18914200	4.34636100
C	2.81112700	-1.37160100	-0.76229400
N	1.42765600	-1.51454800	-0.72546800
C	1.15513400	-2.87349600	-0.79531000
C	2.40905800	-3.61751600	-0.86866000
C	3.42652300	-2.69450400	-0.85688300
C	-0.13538800	-3.44991400	-0.82771700
C	-1.36569200	-2.75557100	-0.87761700
C	-2.67735300	-3.37917300	-1.02734000
C	-3.60238000	-2.36482100	-1.07679300
C	-2.87214100	-1.10501600	-0.94483100
N	-1.51320900	-1.37669500	-0.82357600
C	-3.46568200	0.18196400	-0.97826800
C	-2.75489400	1.40791400	-0.93365800
C	-3.36982100	2.73417500	-0.96306900
C	-2.35353900	3.65609300	-0.89625800
C	-1.10142400	2.90883000	-0.82317900
N	-1.37421400	1.54801500	-0.83735200
C	0.18781900	3.48433500	-0.75395500
C	1.41917000	2.79011300	-0.73903000
C	2.73742600	3.41717900	-0.71985700
C	3.66567000	2.40437700	-0.72303000
C	2.92922100	1.14131600	-0.74584600
N	1.56446800	1.40978200	-0.74383200
C	3.52372300	-0.14593700	-0.75166800
H	4.48671600	-2.88660800	-0.92808300
C	-0.20484100	-4.94912800	-0.81253800
H	-2.86799200	-4.43986100	-1.11071600
H	-4.66982300	-2.45673200	-1.21144400
C	-4.96259800	0.25043600	-1.09113000
H	-4.42999600	2.93038600	-1.02027500
H	-2.44885300	4.73280100	-0.90256500
C	0.25616200	4.98208900	-0.68221900
H	2.93214300	4.48035800	-0.71055800
H	4.74087100	2.50109500	-0.70455000
C	5.02439000	-0.21871200	-0.76970700
H	2.50404400	-4.69139300	-0.94714300
Zn	0.01553900	0.01764500	-0.46641700
C	-0.22501400	-5.65822000	0.40019500
C	-0.29034100	-7.05518400	0.45812800

C	-0.33797800	-7.78941100	-0.73313100
C	-0.31955300	-7.11945300	-1.96219400
C	-0.25376600	-5.71972000	-1.98583800
F	-0.18082300	-4.95677700	1.59806300
F	-0.30880100	-7.71052900	1.67355400
F	-0.40309200	-9.16608500	-0.69487800
F	-0.36593000	-7.84042500	-3.13854100
F	-0.23538500	-5.08898800	-3.21729500
C	0.21116400	5.65086400	0.55241500
C	0.27458500	7.04496500	0.66019900
C	0.38752100	7.81755800	-0.50215300
C	0.43532000	7.18843000	-1.75185800
C	0.36958700	5.79049400	-1.82519400
F	0.22810700	7.66024200	1.89526900
F	0.10173300	4.90943000	1.72161000
F	0.45210000	9.19196800	-0.41520200
F	0.54712600	7.94764000	-2.89947100
F	0.41925500	5.20052700	-3.07589600
C	5.75711600	0.24158500	-1.88895900
C	7.15833300	0.16863300	-1.91212500
C	7.85599800	-0.36146900	-0.80522700
C	7.13454500	-0.82094300	0.31809700
C	5.73405700	-0.75361600	0.33137600
C	-5.78622300	-0.19512400	-0.03099100
C	-7.18464900	-0.12882700	-0.12815800
C	-7.78702400	0.37868000	-1.29957600
C	-6.97403200	0.81988100	-2.36639900
C	-5.57715600	0.75957300	-2.25959000
H	5.18381700	-1.10176300	1.20139300
H	7.68396800	-1.22292600	1.16446600
C	9.34110100	-0.45612600	-0.77827200
H	7.71599100	0.51389800	-2.77601500
H	5.22285700	0.63992000	-2.74726200
H	-4.95617300	1.09091900	-3.08744800
H	-7.45027800	1.20192500	-3.26472900
C	-9.26474200	0.46663500	-1.45382900
H	-7.81305900	-0.46234800	0.69058100
H	-5.32577600	-0.57859200	0.87564000
O	10.01141600	-0.91522900	0.16686000
O	9.92588700	0.02793800	-1.93466700
C	11.39667500	-0.02428300	-2.00502200
H	11.64642400	0.39416700	-2.98096200
H	11.83408500	0.57035700	-1.19689200
O	-9.85398200	0.90567500	-2.46026500
O	-9.94453600	0.00168700	-0.34179900
C	-11.41600500	0.04954800	-0.39853600
H	-11.74758900	-0.35002900	0.56083200
H	-11.75494200	1.08128400	-0.53491300

H	11.74194000	-1.05935800	-1.91927800
H	-11.78138900	-0.56293400	-1.22881400
H	1.84040300	-0.37640600	7.40949200
H	-1.58229100	-1.49063600	7.58199500
O	-0.36996100	1.42028300	7.08645300

Table S3-9. Atomic coordinates of $L3ZnPF_{10}$.

N	0.05075800	0.01735900	1.61505700
C	0.13565400	-1.14997200	2.30670500
C	0.17474100	-1.19340500	3.70777200
C	0.12130400	0.00689300	4.45518500
C	0.03321200	1.21309200	3.72073400
C	0.00132500	1.17959700	2.31937700
C	0.16137000	0.00078500	5.94699600
C	-0.84849900	-0.62283300	6.69593300
C	1.26821800	0.63435600	6.66609000
H	-0.02974400	2.16974000	4.22955900
H	-0.07441900	2.09513300	1.74279900
H	0.18053100	-2.06117800	1.72019000
H	0.25925600	-2.15272000	4.20873600
C	2.78431800	-1.30004300	-1.11083600
N	1.41183400	-1.47731300	-0.97168300
C	1.16887400	-2.84223700	-1.01904500
C	2.43171300	-3.55542500	-1.18796100
C	3.42394100	-2.60739100	-1.25300400
C	-0.10558600	-3.45043500	-0.94488100
C	-1.35325300	-2.78630100	-0.91187000
C	-2.65606000	-3.44531300	-0.88453700
C	-3.60831000	-2.45531200	-0.88121400
C	-2.90234200	-1.17465300	-0.90695600
N	-1.53165600	-1.41009200	-0.91093400
C	-3.52907900	0.09741700	-0.91169600
C	-2.84766500	1.34086900	-0.91901800
C	-3.49545700	2.64858700	-1.01353300
C	-2.50108200	3.59653400	-1.01389500
C	-1.22966800	2.88297300	-0.93423600
N	-1.46896900	1.51780300	-0.87413600
C	0.04689200	3.49086700	-0.94534400
C	1.29390600	2.82686600	-0.99675000
C	2.59538400	3.48613400	-1.05899200
C	3.54582500	2.49633300	-1.12097200
C	2.83994200	1.21559300	-1.09867100
N	1.47217100	1.45072600	-1.00824700
C	3.46468000	-0.05655500	-1.14726700
H	4.47999300	-2.77320600	-1.40570600
C	-0.13349800	-4.94997100	-0.89422500
H	-2.82585800	-4.51275900	-0.87464500

H	-4.68075200	-2.57815300	-0.85727200
C	-5.03102300	0.13196900	-0.93131700
H	-4.55951800	2.81491700	-1.09204500
H	-2.62212500	4.66802600	-1.08999300
C	0.07886100	4.99049500	-0.89691100
H	2.76523200	4.55363700	-1.06123600
H	4.61731600	2.61949200	-1.17084000
C	4.96191700	-0.09133100	-1.26871300
H	2.54669900	-4.62662700	-1.27653000
Zn	-0.01743400	0.02060300	-0.60301100
C	0.06298300	-5.63674400	0.31585400
C	0.04507800	-7.03339900	0.40498700
C	-0.17718400	-7.79167500	-0.75080000
C	-0.37798000	-7.14502400	-1.97603000
C	-0.35409200	-5.74485400	-2.03152500
F	0.27670700	-4.91267900	1.48190300
F	0.24060300	-7.66507300	1.61763200
F	-0.19849900	-9.16854800	-0.68148500
F	-0.59600000	-7.88963800	-3.11794300
F	-0.55080700	-5.13910600	-3.25994600
C	-0.00690500	5.67681400	0.32616300
C	0.01927700	7.07347000	0.41344400
C	0.13532700	7.83183500	-0.75776600
C	0.22356800	7.18543300	-1.99636700
C	0.19488700	5.78526200	-2.04948500
F	-0.06543300	7.70504000	1.63881100
F	-0.11564000	4.95220500	1.50632100
F	0.16300300	9.20862700	-0.69035200
F	0.33706200	7.93003200	-3.15328200
F	0.27989800	5.17922100	-3.29044500
C	5.75848900	-0.61268100	-0.22230700
C	7.15743400	-0.64470900	-0.32788700
C	7.78786600	-0.16127100	-1.49474900
C	7.00203700	0.35505000	-2.54815200
C	5.60510200	0.39291700	-2.43258900
C	-5.75085400	-0.35388900	-2.04826000
C	-7.15346200	-0.31833000	-2.07251700
C	-7.86574700	0.19931100	-0.96901400
C	-7.15736200	0.68484400	0.15168300
C	-5.75561100	0.65490500	0.16590100
H	5.00481800	0.78156000	-3.25068100
H	7.49904000	0.71721600	-3.44347100
C	9.26706600	-0.17664700	-1.65795700
H	7.76514700	-1.03696300	0.48041100
H	5.27680600	-0.97916300	0.68030300
H	-5.21529300	1.02317300	1.03383700
H	-7.71781200	1.07734000	0.99528800
C	-9.35282700	0.25366600	-0.94288200

H	-7.70114000	-0.68334500	-2.93466500
H	-5.20571100	-0.74284400	-2.90398500
O	9.88045500	0.23553500	-2.66127700
O	9.91843400	-0.70695000	-0.55803000
C	11.38923800	-0.76385500	-0.62476900
H	11.69720000	-1.20198600	0.32560700
H	11.70465700	-1.38718300	-1.46735100
O	-10.03581000	0.69967800	-0.00052400
O	-9.92383700	-0.25305200	-2.09647200
C	-11.39546700	-0.24117200	-2.16752300
H	-11.63344700	-0.67496400	-3.13970400
H	-11.81709100	-0.83998000	-1.35410400
H	11.80065800	0.24297800	-0.74715400
H	-11.76853800	0.78496000	-2.09128500
C	2.42373400	1.29403100	5.94244100
O	1.29365800	0.62710800	7.95495100
C	-2.06814800	-1.31084100	6.14675600
O	-0.80962700	-0.63601400	8.04646700
H	0.04290600	-0.13465700	8.35934500
H	3.27517700	1.34916200	6.62572800
H	2.15647100	2.31863700	5.65076000
H	2.70582400	0.75593700	5.03199900
H	-2.94224200	-0.99395500	6.72639800
H	-2.23266300	-1.09744900	5.08960200
H	-1.97355900	-2.39721300	6.27660200

Table S3-10. Atomic coordinates of L4aZnPF$_{10}$.

N	-0.05445000	-0.00551400	1.87819000
C	-0.08220500	-1.19891600	2.52717400
C	-0.13327100	-1.29284000	3.92578100
C	-0.16268400	-0.10661600	4.68936800
C	-0.11865400	1.12942000	4.01451000
C	-0.06859600	1.13879400	2.61286200
H	-0.11803900	2.05400900	4.58102300
H	-0.03863200	2.07209000	2.06182100
H	-0.05606600	-2.09045800	1.91082200
H	-0.11895800	-2.27847500	4.38090900
C	2.81341500	-1.36471600	-0.66445800
N	1.42953900	-1.50360400	-0.63133100
C	1.15288700	-2.86110400	-0.71061200
C	2.40467000	-3.60875400	-0.78623100
C	3.42495100	-2.68885700	-0.76708400
C	-0.13970100	-3.43254600	-0.74874900
C	-1.36754000	-2.73360100	-0.80060800
C	-2.68009800	-3.35156200	-0.96536500

C	-3.60122000	-2.33338300	-1.01498200
C	-2.86772000	-1.07728500	-0.86670500
N	-1.51077600	-1.35482500	-0.73696900
C	-3.45634600	0.21222500	-0.89342600
C	-2.74185000	1.43518300	-0.82912300
C	-3.35188700	2.76387800	-0.85051400
C	-2.33305300	3.68134600	-0.76437500
C	-1.08416800	2.92895000	-0.68789100
N	-1.36169300	1.56948700	-0.71851700
C	0.20677100	3.49981200	-0.60659400
C	1.43584500	2.80147100	-0.59851200
C	2.75659600	3.42338900	-0.56638200
C	3.68090700	2.40743600	-0.58115400
C	2.93961900	1.14749000	-0.62261800
N	1.57601500	1.42087100	-0.62123600
C	3.52987600	-0.14146000	-0.64145700
H	4.48470600	-2.88351400	-0.83798600
C	-0.21520500	-4.93144100	-0.73677700
H	-2.87366100	-4.41077900	-1.06067800
H	-4.66759900	-2.42042200	-1.16103400
C	-4.95165600	0.28754100	-1.02247600
H	-4.41068000	2.96472300	-0.91664500
H	-2.42450800	4.75839400	-0.76185000
C	0.27765800	4.99618500	-0.51379600
H	2.95550900	4.48546100	-0.54023300
H	4.75641000	2.49961200	-0.55767300
C	5.03037600	-0.21859700	-0.65962800
H	2.49664900	-4.68234700	-0.87226500
Zn	0.02188200	0.03157500	-0.35494700
C	-0.26183300	-5.64110300	0.47474400
C	-0.33413900	-7.03758100	0.53172600
C	-0.36156200	-7.77175800	-0.66017400
C	-0.31652500	-7.10158600	-1.88848300
C	-0.24454900	-5.70200600	-1.91081700
F	-0.23762600	-4.94034000	1.67485000
F	-0.37926000	-7.69209100	1.74723900
F	-0.43329900	-9.14801200	-0.62317600
F	-0.34331300	-7.82219400	-3.06543900
F	-0.20077200	-5.07150400	-3.14146200
C	0.15066600	5.65225400	0.72212200
C	0.21196000	7.04486000	0.84894500
C	0.40803200	7.82922100	-0.29427000
C	0.53937900	7.21303900	-1.54440300
C	0.47308300	5.81635400	-1.63732400
F	0.08318800	7.64726400	2.08453300
F	-0.03858900	4.89950700	1.87348100
F	0.47160100	9.20234200	-0.18832200
F	0.73186800	7.98385000	-2.67347200

F	0.60306000	5.23989500	-2.88868500
C	5.76377600	0.24658800	-1.77635900
C	7.16475600	0.16948700	-1.80067600
C	7.86123800	-0.36984800	-0.69752300
C	7.13904700	-0.83353400	0.42357900
C	5.73874100	-0.76184000	0.43810300
C	-5.78980600	-0.16616600	0.02273300
C	-7.18671400	-0.09323800	-0.08999200
C	-7.77324200	0.42951600	-1.26271900
C	-6.94588400	0.87891400	-2.31495700
C	-5.55060300	0.81172100	-2.19241400
H	5.18808900	-1.11214200	1.30698100
H	7.68763600	-1.24164600	1.26754200
C	9.34609400	-0.46985200	-0.67235300
H	7.72310100	0.51868500	-2.66253200
H	5.23027600	0.65232300	-2.63168200
H	-4.91860100	1.14955200	-3.00920900
H	-7.40992000	1.27265500	-3.21462700
C	-9.24869000	0.52535200	-1.43324400
H	-7.82631700	-0.43312000	0.71740900
H	-5.34140300	-0.56148000	0.93033300
O	10.01530300	-0.94071400	0.26766100
O	9.93183400	0.02375800	-1.82425500
C	11.40246900	-0.03192400	-1.89551300
H	11.65325600	0.39669600	-2.86676500
H	11.84169900	0.55236800	-1.08086000
O	-9.82420200	0.97774200	-2.44161700
O	-9.94339800	0.05132800	-0.33423900
C	-11.41397500	0.10604800	-0.40791800
H	-11.75870400	-0.30418900	0.54227500
H	-11.74703600	1.14084300	-0.53524000
H	11.74477300	-1.06888600	-1.82140500
H	-11.77184400	-0.49431300	-1.25021200
C	-0.21269800	-0.08332200	6.18545200
O	0.09531200	0.93579000	6.87647800
N	-0.61181600	-1.21989200	6.82816700
H	-1.01061000	-2.06645600	6.44897500
O	-0.68453700	-1.19748300	8.25411600
H	-0.36837000	-0.28014900	8.48133300

Table S3-11. Atomic coordinates of L4bZnPF$_{10}$.

N	-0.05271800	0.01937700	1.88457400
C	-0.08986900	-1.15785200	2.56893100
C	-0.12721100	-1.21529100	3.96675600
C	-0.12604800	-0.00683800	4.69869100
C	-0.08781000	1.21238500	3.99152900
C	-0.05207700	1.18098800	2.58923300

H	-0.08575100	2.15688700	4.52218300
H	-0.02205200	2.10023200	2.01497000
H	-0.08880400	-2.06517900	1.97522600
H	-0.15621900	-2.17095200	4.47743200
C	2.80485500	-1.37345400	-0.65671400
N	1.42201100	-1.51761800	-0.61857100
C	1.15061000	-2.87629600	-0.69025800
C	2.40518100	-3.61961100	-0.76580200
C	3.42182300	-2.69582700	-0.75310200
C	-0.13947000	-3.45353300	-0.72269400
C	-1.37042500	-2.76002900	-0.76834400
C	-2.68166700	-3.38487100	-0.91853000
C	-3.60776500	-2.37134600	-0.96410200
C	-2.87815200	-1.11108900	-0.82981900
N	-1.51927500	-1.38176600	-0.71027500
C	-3.47261300	0.17564100	-0.86245600
C	-2.76270500	1.40228200	-0.82098300
C	-3.37876000	2.72824200	-0.85360700
C	-2.36279400	3.65085300	-0.79224100
C	-1.11015700	2.90411000	-0.71860800
N	-1.38228300	1.54349100	-0.72717800
C	0.17900700	3.48072700	-0.65562400
C	1.41082300	2.78736500	-0.64156900
C	2.72895700	3.41556300	-0.62579100
C	3.65758200	2.40329900	-0.62657600
C	2.92122500	1.13974800	-0.64471100
N	1.55667100	1.40746600	-0.64212600
C	3.51640500	-0.14712000	-0.64772500
H	4.48221200	-2.88677600	-0.82488700
C	-0.20775300	-4.95295600	-0.71578900
H	-2.87125900	-4.44555400	-1.00486400
H	-4.67520000	-2.46405500	-1.09848700
C	-4.96972200	0.24256800	-0.97263700
H	-4.43911300	2.92389400	-0.90972000
H	-2.45861500	4.72753400	-0.80295900
C	0.24610900	4.97886500	-0.59100000
H	2.92322100	4.47887900	-0.61930600
H	4.73277100	2.50043800	-0.60882000
C	5.01711500	-0.21925200	-0.66507800
H	2.50095000	-4.69335600	-0.84563500
Zn	0.00881800	0.01405800	-0.33600800
C	-0.22883200	-5.67040100	0.49209800
C	-0.29304900	-7.06792100	0.54002800
C	-0.33854200	-7.79418900	-0.65604000
C	-0.31914600	-7.11584000	-1.88038200
C	-0.25454100	-5.71593900	-1.89429300
F	-0.18676500	-4.97834200	1.69498600
F	-0.31256800	-7.73181400	1.75113400

F	-0.40259600	-9.17141500	-0.62724200
F	-0.36346500	-7.82900400	-3.06182300
F	-0.23528000	-5.07734300	-3.12171100
C	0.17473800	5.65607200	0.63793100
C	0.23571300	7.05096900	0.73733700
C	0.37358100	7.81611800	-0.42704700
C	0.44822400	7.17865700	-1.67109900
C	0.38408400	5.78023600	-1.73645000
F	0.16267600	7.67458300	1.96749300
F	0.04159600	4.92400300	1.81018200
F	0.43601200	9.19138900	-0.34763700
F	0.58414700	7.93047400	-2.82122700
F	0.45936800	5.18286700	-2.98233500
C	5.75043900	0.23784100	-1.78528500
C	7.15163100	0.16488100	-1.80764300
C	7.84886900	-0.36211400	-0.69890000
C	7.12680800	-0.81812300	0.42553100
C	5.72632000	-0.75072900	0.43798800
C	-5.79109700	-0.20838100	0.08710800
C	-7.18975100	-0.14423400	-0.00722300
C	-7.79529300	0.36682100	-1.17555100
C	-6.98477700	0.81333400	-2.24213400
C	-5.58765700	0.75484300	-2.13806100
H	5.17548800	-1.09570000	1.30886200
H	7.67569100	-1.21736200	1.27354800
C	9.33368900	-0.45694300	-0.67130800
H	7.70963700	0.50767800	-2.67230000
H	5.21641800	0.63370800	-2.64487200
H	-4.96868700	1.08982400	-2.96592700
H	-7.46316400	1.19773800	-3.13832600
C	-9.27312200	0.45266200	-1.32684900
H	-7.81612600	-0.48234000	0.81122300
H	-5.32796600	-0.59475900	0.99111200
O	10.00435200	-0.91389800	0.27471100
O	9.91920900	0.02437300	-1.82892500
C	11.38981300	-0.02854800	-1.89820600
H	11.64037700	0.38708900	-2.87517300
H	11.82709900	0.56816200	-1.09150100
O	-9.86558300	0.89461700	-2.33019500
O	-9.95062600	-0.01812700	-0.21534000
C	-11.42208600	0.02652900	-0.27072000
H	-11.75207900	-0.37794000	0.68718500
H	-11.76375200	1.05798500	-0.40252500
H	11.73486800	-1.06345700	-1.80932500
H	-11.78686000	-0.58322400	-1.10329100
C	-0.16334800	-0.00742400	6.17362500
O	-0.15911600	1.23149900	6.77206200
N	-0.19731600	-1.13768500	6.83900700

O	-0.22786100	-0.80988600	8.26495700
H	-0.24894100	-1.67802100	8.71602700
H	-0.18361700	1.13415000	7.75277900

Table S3-12. Atomic coordinates of $L5ZnPF_{10}$.

N	0.04961000	-0.03124900	2.00745900
C	0.08867600	1.13485500	2.70709300
C	0.11807400	1.16618500	4.10958000
C	0.10691300	-0.04458500	4.84122200
C	0.06662700	-1.24825800	4.09932800
C	0.03916400	-1.20379500	2.69698700
H	0.05623400	-2.20599500	4.60885600
H	0.00768800	-2.11392000	2.10784300
H	0.09548400	2.05001100	2.12464400
H	0.14872000	2.11897300	4.62759200
C	-2.79818800	1.38831600	-0.53205800
N	-1.41566400	1.53195300	-0.49168600
C	-1.14400900	2.89073700	-0.55552700
C	-2.39836800	3.63495600	-0.62832100
C	-3.41518400	2.71140200	-0.62113900
C	0.14607600	3.46799300	-0.58304300
C	1.37705000	2.77459500	-0.62742700
C	2.68880800	3.40053700	-0.76942800
C	3.61520000	2.38741800	-0.81616800
C	2.88482300	1.12638200	-0.69172000
N	1.52576000	1.39626200	-0.57581000
C	3.47932600	-0.16018700	-0.73145100
C	2.76906800	-1.38703100	-0.70478900
C	3.38516000	-2.71286500	-0.74818900
C	2.36860100	-3.63563700	-0.70220100
C	1.11587900	-2.88897000	-0.62667500
N	1.38839000	-1.52866600	-0.61919100
C	-0.17359100	-3.46589700	-0.57556000
C	-1.40520700	-2.77241200	-0.55596400
C	-2.72342900	-3.40084000	-0.55021200
C	-3.65195300	-2.38856900	-0.54017900
C	-2.91515700	-1.12496200	-0.54257400
N	-1.55085300	-1.39280300	-0.54059500
C	-3.50997200	0.16204200	-0.53330600
H	-4.47552200	2.90294100	-0.69239400
C	0.21447600	4.96748200	-0.57420300
H	2.87849400	4.46172600	-0.84937300
H	4.68319300	2.48093700	-0.94559900
C	4.97697100	-0.22599000	-0.83370700
H	4.44575300	-2.90833000	-0.80044800
H	2.46402300	-4.71222100	-0.72349600
C	-0.24160100	-4.96483400	-0.53248200

H	-2.91769600	-4.46419100	-0.55657200
H	-4.72717400	-2.48583300	-0.52492800
C	-5.01058900	0.23510200	-0.54865400
H	-2.49377200	4.70919600	-0.70199700
Zn	-0.00325600	-0.00243200	-0.20438200
C	0.23611000	5.68488100	0.63378300
C	0.30051300	7.08253700	0.68126000
C	0.34559900	7.80884800	-0.51468300
C	0.32564000	7.13053000	-1.73895500
C	0.26087400	5.73067500	-1.75269600
F	0.19432600	4.99369100	1.83656800
F	0.32056000	7.74681900	1.89234800
F	0.40982300	9.18629700	-0.48588800
F	0.36959900	7.84383200	-2.92057300
F	0.24119800	5.09238500	-2.98033500
C	-0.18846500	-5.66026700	0.68725000
C	-0.25102900	-7.05660900	0.76454900
C	-0.37157800	-7.80444400	-0.41280200
C	-0.42768200	-7.14853600	-1.64812500
C	-0.36250700	-5.74931200	-1.69156700
F	-0.19605200	-7.69869100	1.98643200
F	-0.07191800	-4.94686100	1.87220900
F	-0.43524800	-9.18097500	-0.35473900
F	-0.54663100	-7.88325200	-2.81133500
F	-0.41962900	-5.13384100	-2.92961500
C	-5.74620000	-0.21280700	-1.67111400
C	-7.14733900	-0.13849800	-1.69080100
C	-7.84253900	0.38062000	-0.57699700
C	-7.11821700	0.82755700	0.54969500
C	-5.71781300	0.75893600	0.55942300
C	5.79199100	0.21960400	0.23328200
C	7.19117700	0.15720300	0.14669800
C	7.80405300	-0.34680000	-1.02095000
C	7.00000400	-0.78795900	-2.09470400
C	5.60229000	-0.73110400	-1.99839000
H	-5.16503100	1.09697400	1.43176600
H	-7.66537700	1.22095400	1.40155800
C	-9.32699600	0.47634700	-0.54633400
H	-7.70689100	-0.47416800	-2.55727100
H	-5.21377000	-0.60246400	-2.53450600
H	4.98836300	-1.06162000	-2.83177200
H	7.48381700	-1.16681100	-2.99035800
C	9.28256300	-0.43030400	-1.16421000
H	7.81245900	0.49141100	0.97062400
H	5.32302400	0.60049800	1.13658300
O	-9.99641400	0.92483300	0.40474300
O	-9.91490100	0.00639000	-1.70771400
C	-11.38538800	0.06160700	-1.77407900

H	-11.63797400	-0.34319000	-2.75509200
H	-11.82218800	-0.54332400	-0.97322100
O	9.88181100	-0.86588500	-2.16639300
O	9.95356500	0.03494500	-0.04601300
C	11.42518100	-0.00756100	-0.09410900
H	11.74981000	0.39106100	0.86810600
H	11.76900500	-1.03766400	-0.23095900
H	-11.72934000	1.09582500	-1.67346200
H	11.79360100	0.60807400	-0.92075100
B	0.13638200	-0.05180800	6.40412100
O	0.17469100	1.17236400	7.04479200
O	0.12170700	-1.28155700	7.03458500
H	0.13550000	-1.40515200	7.99867300
H	0.19338400	1.28654800	8.00998300

Table S3-13. Atomic coordinates of L1-anatase101-M.

Ti	0.63392	15.30531	8.45636
Ti	3.44428	0.08972	7.84637
Ti	5.86697	1.97745	8.47463
Ti	8.68476	2.03056	7.89409
Ti	0.61201	3.91279	8.46258
Ti	0.66466	7.73907	8.50505
Ti	0.65200	11.50339	8.50068
Ti	3.41390	3.85056	7.84803
Ti	3.47901	7.74540	7.86787
Ti	3.47052	11.49696	7.89325
Ti	5.76548	5.73618	8.39093
Ti	5.88083	9.60983	8.73694
Ti	5.89946	13.40451	8.48108
Ti	8.71888	5.87602	7.85821
Ti	8.65286	9.64757	7.85534
Ti	8.70799	13.41392	7.89856
O	10.56332	2.04079	8.69353
O	3.85735	0.02282	5.74898
O	2.27038	15.34220	9.30666
O	1.59137	15.24387	6.90091
O	5.32297	15.30657	8.70379
O	9.10395	1.94856	5.77415
O	7.49906	2.03931	9.34539
O	3.88943	1.97926	7.82948
O	6.84180	1.95362	6.92128
O	9.12118	15.32555	7.92779
O	10.55335	5.81728	8.70492
O	10.62106	9.62047	8.63336
O	10.58386	13.43305	8.70684
O	3.85291	3.84013	5.74601
O	3.85726	7.63694	5.82569
O	3.85871	11.42616	5.82936

O	2.25176	3.90475	9.31444
O	2.28527	7.71979	9.36018
O	2.27971	11.53018	9.36918
O	1.57656	3.84226	6.90681
O	1.58951	7.64159	6.94392
O	1.60967	11.51328	6.95017
O	5.29851	3.85915	8.71723
O	5.32874	7.64347	8.51080
O	5.37930	11.52467	8.61683
O	9.11158	5.74546	5.82866
O	9.13154	9.53122	5.83184
O	9.11208	13.33242	5.80921
O	7.35865	6.07978	9.44532
O	7.63130	9.64139	9.39130
O	7.51526	13.43680	9.36801
O	3.86195	5.74479	7.84470
O	3.84832	9.60928	7.94212
O	3.88315	13.40652	7.93072
O	6.86495	5.63703	6.95073
O	6.86345	9.54734	7.02058
O	6.86285	13.42038	6.93782
O	9.07369	3.94340	7.95138
O	9.11805	7.70239	7.94777
O	9.13344	11.53154	7.93574
O	6.43325	7.52053	11.40843
C	5.68446	8.55532	11.59494
C	5.17367	8.95269	12.95850
O	5.29919	9.36187	10.60035
C	5.27922	8.07480	14.06957
C	4.58099	10.22874	13.16619
C	4.80924	8.51213	15.33083
H	5.72446	7.07090	13.94353
C	4.16169	10.58228	14.47204
H	4.46292	10.93409	12.32265
H	4.88038	7.85193	16.21712
H	3.73124	11.58494	14.67241
N	4.26493	9.75138	15.55322
H	7.14026	6.76225	10.26797
Ti	1.95273	-0.03160	4.88410
Ti	4.87400	-0.02149	4.19308
Ti	7.19495	1.89800	4.92578
Ti	10.10811	1.89800	4.19733
Ti	1.95273	3.82760	4.88410
Ti	1.96603	7.62556	4.95841
Ti	1.96603	11.35444	4.95841
Ti	4.87400	3.81749	4.19308
Ti	4.88673	7.59140	4.26667
Ti	4.88673	11.38860	4.26667

Ti	7.20627	5.69554	4.92413
Ti	7.20629	9.49000	4.96097
Ti	7.20627	13.28446	4.92413
Ti	10.12802	5.69422	4.23725
Ti	10.13103	9.49000	4.28219
Ti	10.12802	13.28578	4.23725
O	1.50815	1.89800	4.85674
O	0.09219	-0.03407	4.08191
O	3.11924	-0.02997	3.25583
O	6.76373	-0.03578	4.87464
O	5.36212	1.89800	4.08511
O	8.34378	1.89800	3.28133
O	1.52660	5.69312	4.91841
O	1.53166	9.49000	4.98906
O	1.52660	13.28688	4.91841
O	0.09219	3.83007	4.08191
O	0.12587	7.62602	4.12486
O	0.12587	11.35398	4.12486
O	3.11924	3.82597	3.25583
O	3.12760	7.62092	3.32997
O	3.12760	11.35908	3.32997
O	6.76373	3.83178	4.87464
O	6.76248	7.62102	4.98540
O	6.76248	11.35898	4.98540
O	5.36629	5.74107	4.08249
O	5.39119	9.49000	4.07365
O	5.36629	13.23893	4.08249
O	8.37288	5.74079	3.29848
O	8.37941	9.49000	3.33900
O	8.37288	13.23921	3.29848

Table S3-14. Atomic coordinates of L1-anatase101-B.

Ti	0.59251	15.24320	8.41083
Ti	3.40345	0.09139	7.84939
Ti	5.85937	1.94019	8.43619
Ti	8.67647	1.96357	7.84203
Ti	0.62177	3.86437	8.40493
Ti	0.64453	7.56442	8.48308
Ti	0.63122	11.47311	8.49252
Ti	3.45593	3.84465	7.82444
Ti	3.44429	7.54031	7.86523
Ti	3.41433	11.53492	7.87463
Ti	5.82141	5.71955	8.90880
Ti	5.61227	9.53660	8.46674
Ti	5.85485	13.37057	8.46207
Ti	8.56658	5.71537	7.81617
Ti	8.85532	9.51408	7.78540
Ti	8.67337	13.33935	7.90340

O	10.55787	1.94297	8.60677
O	3.86187	0.03069	5.74608
O	2.21541	15.28208	9.29523
O	1.57667	15.21772	6.87360
O	5.28741	15.24013	8.67764
O	9.10170	1.92494	5.76365
O	7.48567	1.94428	9.29936
O	3.83344	1.94042	7.83067
O	6.82857	1.91618	6.88190
O	9.08430	15.22465	7.85705
O	10.57850	5.72457	8.62666
O	10.69800	9.54076	8.52753
O	10.54590	13.35582	8.72322
O	3.86062	3.82449	5.74494
O	3.85930	7.64069	5.82779
O	3.85581	11.40597	5.83278
O	2.25271	3.84145	9.27686
O	2.26292	7.62442	9.35639
O	2.25711	11.53003	9.36752
O	1.59413	3.83761	6.86220
O	1.60019	7.54578	6.93263
O	1.57731	11.51547	6.93883
O	5.32657	3.78059	8.60836
O	5.34336	7.64631	8.52681
O	5.29776	11.49816	8.60581
O	9.13114	5.72870	5.77074
O	9.12159	9.53471	5.84596
O	9.10760	13.28325	5.80972
O	7.62813	5.74870	9.40000
O	7.47077	13.33970	9.36509
O	3.85166	5.72036	7.90384
O	3.79501	9.55374	7.93698
O	3.82847	13.37344	7.85465
O	6.85820	5.69493	6.97417
O	6.93832	9.53452	7.17484
O	6.83772	13.34926	6.93317
O	9.09188	3.83176	7.86149
O	9.11161	7.65120	7.94487
O	9.13075	11.44321	7.94204
O	8.39211	9.60328	9.86086
C	7.43651	9.62631	10.74038
C	7.69128	9.65764	12.20583
O	6.16541	9.61571	10.36233
C	9.00844	9.66812	12.73368
C	6.58980	9.65811	13.09562
C	9.15615	9.67310	14.13841
H	9.88393	9.66884	12.06397
C	6.84583	9.66430	14.48340

H	5.55592	9.65073	12.70458
H	10.16739	9.67735	14.59351
H	6.01234	9.66280	15.21094
N	8.10902	9.66976	15.02218
O	5.21494	5.73951	10.61450
H	5.35141	5.55163	11.57487
Ti	1.95273	-0.03160	4.88410
Ti	4.87400	-0.02149	4.19308
Ti	7.19495	1.89800	4.92578
Ti	10.10811	1.89800	4.19733
Ti	1.95273	3.82760	4.88410
Ti	1.96603	7.62556	4.95841
Ti	1.96603	11.35444	4.95841
Ti	4.87400	3.81749	4.19308
Ti	4.88673	7.59140	4.26667
Ti	4.88673	11.38860	4.26667
Ti	7.20627	5.69554	4.92413
Ti	7.20629	9.49000	4.96097
Ti	7.20627	13.28446	4.92413
Ti	10.12802	5.69422	4.23725
Ti	10.13103	9.49000	4.28219
Ti	10.12802	13.28578	4.23725
O	1.50815	1.89800	4.85674
O	0.09219	-0.03407	4.08191
O	3.11924	-0.02997	3.25583
O	6.76373	-0.03578	4.87464
O	5.36212	1.89800	4.08511
O	8.34378	1.89800	3.28133
O	1.52660	5.69312	4.91841
O	1.53166	9.49000	4.98906
O	1.52660	13.28688	4.91841
O	0.09219	3.83007	4.08191
O	0.12587	7.62602	4.12486
O	0.12587	11.35398	4.12486
O	3.11924	3.82597	3.25583
O	3.12760	7.62092	3.32997
O	3.12760	11.35908	3.32997
O	6.76373	3.83178	4.87464
O	6.76248	7.62102	4.98540
O	6.76248	11.35898	4.98540
O	5.36629	5.74107	4.08249
O	5.39119	9.49000	4.07365
O	5.36629	13.23893	4.08249
O	8.37288	5.74079	3.29848
O	8.37941	9.49000	3.33900
O	8.37288	13.23921	3.29848

Table S3-15. Atomic coordinates of L2-anatase101-M.

Ti	0.67260	15.29982	8.44654
Ti	3.48307	0.12564	7.83505
Ti	5.89437	2.01287	8.46763
Ti	8.72350	2.02513	7.87364
Ti	0.65490	3.91793	8.44483
Ti	0.66646	7.73729	8.50298
Ti	0.68296	11.50035	8.51130
Ti	3.46286	3.91083	7.82476
Ti	3.54235	7.75659	7.82201
Ti	3.50221	11.51254	7.90221
Ti	5.86029	5.76854	8.42360
Ti	5.92162	9.64563	8.78992
Ti	5.92457	13.43012	8.48521
Ti	8.71954	5.85367	7.92260
Ti	8.68314	9.63598	7.85718
Ti	8.73869	13.41028	7.89675
O	10.61379	2.03567	8.64616
O	3.87275	0.03121	5.74808
O	2.30925	15.34851	9.29293
O	1.62816	15.22873	6.89299
O	5.35193	15.33313	8.70057
O	9.11077	1.94690	5.77209
O	7.53299	2.03272	9.32219
O	3.92042	2.02482	7.81852
O	6.86257	1.95479	6.91399
O	9.15199	15.31917	7.92283
O	10.59935	5.82415	8.71176
O	10.64898	9.62120	8.70444
O	10.62891	13.42959	8.70257
O	3.86505	3.85462	5.74308
O	3.86495	7.65038	5.82611
O	3.87287	11.43388	5.82826
O	2.29555	3.94733	9.29065
O	2.34067	7.72274	9.37677
O	2.31521	11.52218	9.37279
O	1.60147	3.84233	6.88553
O	1.61537	7.64087	6.95826
O	1.63951	11.48428	6.95604
O	5.33138	3.90360	8.70237
O	5.33389	7.65854	8.65646
O	5.40893	11.53859	8.62991
O	9.12603	5.73922	5.81861
O	9.13331	9.53695	5.83161
O	9.12264	13.33565	5.80964
O	7.45495	5.95630	9.39511
O	7.65041	9.64778	9.40834
O	7.54406	13.43847	9.36769
O	3.89974	5.79212	7.83333

O 3.90366 9.61639 7.93622
O 3.91135 13.42428 7.93291
O 6.89816 5.72529 6.93818
O 6.88212 9.51933 7.04922
O 6.89033 13.42062 6.94124
O 9.12158 3.93789 7.94255
O 9.17623 7.72235 7.94547
O 9.16776 11.52588 7.93461
O 3.67071 7.30572 11.41242
C 4.96741 8.49140 13.52900
O 5.26384 9.52927 10.71461
C 4.07985 7.63862 14.24163
C 5.67570 9.49789 14.22423
C 3.95071 7.82595 15.63400
H 3.50178 6.86391 13.71363
C 5.46104 9.60728 15.61479
H 6.36910 10.18902 13.70357
H 3.27883 7.17228 16.22130
H 5.99072 10.38904 16.20784
N 4.62093 8.79823 16.33151
O 6.49322 7.13262 11.63038
H 6.90396 6.76382 10.74291
P 5.10977 8.17561 11.70676
H 3.05634 7.53161 10.53463
Ti 1.95273 -0.03160 4.88410
Ti 4.87400 -0.02149 4.19308
Ti 7.19495 1.89800 4.92578
Ti 10.10811 1.89800 4.19733
Ti 1.95273 3.82760 4.88410
Ti 1.96603 7.62556 4.95841
Ti 1.96603 11.35444 4.95841
Ti 4.87400 3.81749 4.19308
Ti 4.88673 7.59140 4.26667
Ti 4.88673 11.38860 4.26667
Ti 7.20627 5.69554 4.92413
Ti 7.20629 9.49000 4.96097
Ti 7.20627 13.28446 4.92413
Ti 10.12802 5.69422 4.23725
Ti 10.13103 9.49000 4.28219
Ti 10.12802 13.28578 4.23725
O 1.50815 1.89800 4.85674
O 0.09219 -0.03407 4.08191
O 3.11924 -0.02997 3.25583
O 6.76373 -0.03578 4.87464
O 5.36212 1.89800 4.08511
O 8.34378 1.89800 3.28133
O 1.52660 5.69312 4.91841
O 1.53166 9.49000 4.98906

O 1.52660 13.28688 4.91841
O 0.09219 3.83007 4.08191
O 0.12587 7.62602 4.12486
O 0.12587 11.35398 4.12486
O 3.11924 3.82597 3.25583
O 3.12760 7.62092 3.32997
O 3.12760 11.35908 3.32997
O 6.76373 3.83178 4.87464
O 6.76248 7.62102 4.98540
O 6.76248 11.35898 4.98540
O 5.36629 5.74107 4.08249
O 5.39119 9.49000 4.07365
O 5.36629 13.23893 4.08249
O 8.37288 5.74079 3.29848
O 8.37941 9.49000 3.33900
O 8.37288 13.23921 3.29848

Table S3-16. Atomic coordinates of L2-anatase101-B.

Ti 0.62956 15.27097 8.48256
Ti 3.41722 0.16410 7.84636
Ti 5.90729 2.02672 8.41354
Ti 8.73194 1.99076 7.81988
Ti 0.64764 3.85780 8.40630
Ti 0.57320 7.61201 8.46331
Ti 0.51466 11.45891 8.40336
Ti 3.46022 3.89758 7.82585
Ti 3.38915 7.58600 7.88941
Ti 3.46633 11.58300 7.72717
Ti 5.88857 5.78077 8.92058
Ti 5.61287 9.60529 8.44631
Ti 5.87848 13.45717 8.40230
Ti 8.58355 5.67826 7.77352
Ti 8.67241 9.52342 7.78928
Ti 8.68122 13.40156 7.83606
O 10.56005 1.94190 8.67873
O 3.86021 -0.05734 5.74942
O 2.24895 15.33645 9.35132
O 1.58792 15.23961 6.91857
O 5.33887 15.30963 8.66877
O 9.10232 1.86705 5.74595
O 7.52176 2.03010 9.27238
O 3.88046 1.95986 7.80755
O 6.85790 1.91999 6.86877
O 9.14766 15.21537 7.82101
O 10.60112 5.73564 8.60113
O 10.51467 9.60997 8.72595
O 10.54953 13.32890 8.72868
O 3.86678 3.83327 5.73079

O 3.79709 7.63915 5.84317
O 3.82598 11.45547 5.82490
O 2.26421 3.80142 9.28140
O 2.16872 7.72943 9.32464
O 2.24275 11.51266 9.40099
O 1.60391 3.81009 6.84743
O 1.48881 7.63883 6.89955
O 1.55985 11.50105 6.96358
O 5.31904 3.83620 8.52836
O 5.29815 7.70624 8.39842
O 5.31600 11.54703 8.35339
O 9.12960 5.75712 5.77388
O 9.12743 9.50753 5.84086
O 9.10728 13.31624 5.79950
O 7.64644 5.28445 9.27585
O 7.48185 13.32021 9.29724
O 3.70190 5.76180 7.85030
O 3.72244 9.64237 7.88620
O 3.81688 13.44135 7.93389
O 6.87398 5.76866 6.96247
O 6.87482 9.52212 6.99309
O 6.84420 13.43897 6.86800
O 9.21510 3.80208 7.69612
O 9.00446 7.65449 8.03794
O 9.15568 11.48454 7.78212
O 5.41562 9.55171 10.46207
C 8.08082 9.30498 12.28672
O 7.56431 9.84850 9.35905
C 7.68361 9.22829 13.61260
C 9.45941 9.24474 11.94734
C 8.64789 9.02458 14.60517
H 6.60375 9.26221 13.91781
C 10.38184 9.00124 13.03071
H 9.81418 9.31226 10.93145
H 8.37168 8.92854 15.64471
H 11.40736 8.87088 12.77983
N 9.99791 8.85853 14.30846
O 7.19853 7.31440 10.58500
O 4.98421 5.85875 10.47521
H 4.91967 6.37245 11.32932
P 7.00383 8.91734 10.77758
H 2.63456 11.29366 10.28184
Ti 1.95273 -0.03160 4.88410
Ti 4.87400 -0.02149 4.19308
Ti 7.19495 1.89800 4.92578
Ti 10.10811 1.89800 4.19733
Ti 1.95273 3.82760 4.88410
Ti 1.96603 7.62556 4.95841

Ti	1.96603	11.35444	4.95841
Ti	4.87400	3.81749	4.19308
Ti	4.88673	7.59140	4.26667
Ti	4.88673	11.38860	4.26667
Ti	7.20627	5.69554	4.92413
Ti	7.20629	9.49000	4.96097
Ti	7.20627	13.28446	4.92413
Ti	10.12802	5.69422	4.23725
Ti	10.13103	9.49000	4.28219
Ti	10.12802	13.28578	4.23725
O	1.50815	1.89800	4.85674
O	0.09219	-0.03407	4.08191
O	3.11924	-0.02997	3.25583
O	6.76373	-0.03578	4.87464
O	5.36212	1.89800	4.08511
O	8.34378	1.89800	3.28133
O	1.52660	5.69312	4.91841
O	1.53166	9.49000	4.98906
O	1.52660	13.28688	4.91841
O	0.09219	3.83007	4.08191
O	0.12587	7.62602	4.12486
O	0.12587	11.35398	4.12486
O	3.11924	3.82597	3.25583
O	3.12760	7.62092	3.32997
O	3.12760	11.35908	3.32997
O	6.76373	3.83178	4.87464
O	6.76248	7.62102	4.98540
O	6.76248	11.35898	4.98540
O	5.36629	5.74107	4.08249
O	5.39119	9.49000	4.07365
O	5.36629	13.23893	4.08249
O	8.37288	5.74079	3.29848
O	8.37941	9.49000	3.33900
O	8.37288	13.23921	3.29848

Table S3-17. Atomic coordinates of L5-anatase101-M.

Ti	0.69634	15.29435	8.46942
Ti	3.50374	0.10208	7.84394
Ti	5.93111	1.98679	8.45990
Ti	8.76003	2.03517	7.88084
Ti	0.70147	3.91159	8.47633
Ti	0.72852	7.73237	8.51355
Ti	0.65668	11.48009	8.49204
Ti	3.49962	3.88970	7.84343
Ti	3.59613	7.69574	7.87630
Ti	3.65617	11.45266	7.82027
Ti	5.96410	5.75102	8.49110
Ti	5.97392	9.57606	8.91117

Ti	5.96448	13.43162	8.48523
Ti	8.78609	5.83334	7.88288
Ti	8.69097	9.58800	7.82097
Ti	8.77941	13.42181	7.87915
O	10.64122	2.02319	8.70050
O	3.87451	0.01823	5.74706
O	2.34292	15.34797	9.30885
O	1.64342	15.22330	6.91167
O	5.38728	15.31168	8.70062
O	9.12455	1.94079	5.76836
O	7.57563	2.05027	9.31727
O	3.94494	1.98167	7.81626
O	6.90355	1.93472	6.91149
O	9.18747	15.30879	7.91439
O	10.68190	5.81582	8.68938
O	10.68499	9.61889	8.71567
O	10.66401	13.41385	8.72243
O	3.87445	3.84918	5.74319
O	3.88327	7.63702	5.82638
O	3.87835	11.42572	5.83484
O	2.34654	3.92657	9.31344
O	2.39944	7.84329	9.39918
O	2.38042	11.33502	9.49124
O	1.64564	3.84562	6.91231
O	1.68030	7.64103	6.97231
O	1.69870	11.52338	7.01274
O	5.38634	3.85445	8.69842
O	5.42736	7.63068	8.64150
O	5.45180	11.53892	8.60770
O	9.13102	5.73639	5.80903
O	9.14876	9.53261	5.82264
O	9.12714	13.33667	5.80466
O	7.59993	5.84181	9.35335
O	7.74729	9.64902	9.40776
O	7.60195	13.41840	9.34771
O	3.93666	5.76413	7.91581
O	3.99295	9.58965	7.92727
O	3.93560	13.38940	7.94017
O	6.91757	5.72485	6.94028
O	6.93190	9.53997	7.04235
O	6.92006	13.43371	6.93611
O	9.19074	3.92083	7.92172
O	9.24818	7.70834	7.92647
O	9.26233	11.51744	7.86155
O	3.05038	9.41670	11.47258
C	4.98242	9.82957	13.17502
O	5.26502	9.62524	10.60306
C	4.06557	9.85602	14.26907

C 6.36262 9.98061 13.50303
C 4.54071 10.04061 15.58356
H 2.99041 9.72679 14.06751
C 6.75004 10.14492 14.85146
H 7.14296 9.96229 12.71236
H 3.82599 10.07236 16.43570
H 7.82191 10.25307 15.13622
N 5.86719 10.18270 15.90624
B 4.44406 9.60463 11.72092
H 2.81053 8.76160 10.70396
H 2.63076 10.79741 10.33781
Ti 1.95273 -0.03160 4.88410
Ti 4.87400 -0.02149 4.19308
Ti 7.19495 1.89800 4.92578
Ti 10.10811 1.89800 4.19733
Ti 1.95273 3.82760 4.88410
Ti 1.96603 7.62556 4.95841
Ti 1.96603 11.35444 4.95841
Ti 4.87400 3.81749 4.19308
Ti 4.88673 7.59140 4.26667
Ti 4.88673 11.38860 4.26667
Ti 7.20627 5.69554 4.92413
Ti 7.20629 9.49000 4.96097
Ti 7.20627 13.28446 4.92413
Ti 10.12802 5.69422 4.23725
Ti 10.13103 9.49000 4.28219
Ti 10.12802 13.28578 4.23725
O 1.50815 1.89800 4.85674
O 0.09219 -0.03407 4.08191
O 3.11924 -0.02997 3.25583
O 6.76373 -0.03578 4.87464
O 5.36212 1.89800 4.08511
O 8.34378 1.89800 3.28133
O 1.52660 5.69312 4.91841
O 1.53166 9.49000 4.98906
O 1.52660 13.28688 4.91841
O 0.09219 3.83007 4.08191
O 0.12587 7.62602 4.12486
O 0.12587 11.35398 4.12486
O 3.11924 3.82597 3.25583
O 3.12760 7.62092 3.32997
O 3.12760 11.35908 3.32997
O 6.76373 3.83178 4.87464
O 6.76248 7.62102 4.98540
O 6.76248 11.35898 4.98540
O 5.36629 5.74107 4.08249
O 5.39119 9.49000 4.07365
O 5.36629 13.23893 4.08249

O 8.37288 5.74079 3.29848
O 8.37941 9.49000 3.33900
O 8.37288 13.23921 3.29848

Table S3-18. Atomic coordinates of L5-anatase101-M.

Ti 0.60572 15.24983 8.44490
Ti 3.40829 0.07530 7.84866
Ti 5.86034 1.93649 8.43678
Ti 8.68787 1.98386 7.85770
Ti 0.62267 3.88824 8.41559
Ti 0.61957 7.60058 8.49493
Ti 0.51022 11.40522 8.41002
Ti 3.44789 3.84728 7.81439
Ti 3.44370 7.57195 7.87235
Ti 3.53110 11.48011 7.77734
Ti 5.76510 5.69568 8.95729
Ti 5.68693 9.49323 8.67401
Ti 5.87243 13.38155 8.47671
Ti 8.53369 5.73562 7.81093
Ti 8.64488 9.48580 7.82459
Ti 8.68194 13.36775 7.88115
O 10.57113 1.95063 8.60870
O 3.85495 -0.03670 5.74889
O 2.23483 15.23991 9.31570
O 1.57718 15.22824 6.89483
O 5.29255 15.23615 8.69714
O 9.10642 1.92529 5.77083
O 7.48714 1.94726 9.30134
O 3.84120 1.92213 7.82273
O 6.84037 1.90803 6.88525
O 9.09429 15.23027 7.91994
O 10.58715 5.74364 8.63349
O 10.57560 9.54856 8.71102
O 10.55154 13.32958 8.70906
O 3.85583 3.83361 5.74342
O 3.84321 7.63801 5.82744
O 3.85889 11.43142 5.83714
O 2.25723 3.84105 9.27883
O 2.25739 7.63985 9.36251
O 2.24198 11.44636 9.39899
O 1.58452 3.83562 6.86384
O 1.58176 7.63200 6.94470
O 1.60264 11.43278 6.96002
O 5.30774 3.76567 8.60324
O 5.32615 7.63753 8.58552
O 5.29980 11.51091 8.60901
O 9.13728 5.73188 5.78855

O	9.12153	9.52319	5.84302
O	9.10203	13.32991	5.80592
O	7.54950	5.74573	9.39632
O	7.49285	13.32974	9.35683
O	3.81389	5.72482	7.89556
O	3.86181	9.56138	7.94819
O	3.81392	13.34873	7.92155
O	6.84677	5.68956	6.95960
O	6.86931	9.53977	7.07448
O	6.83428	13.35057	6.92950
O	9.09328	3.84483	7.90640
O	9.09090	7.65176	7.94266
O	9.14741	11.44313	7.83704
O	7.70396	9.63538	9.50934
C	7.79503	9.77822	12.15101
O	5.67125	9.64027	10.60447
C	9.21425	9.80879	12.23801
C	7.06924	9.83227	13.37440
C	9.83245	9.89831	13.50390
H	9.83145	9.75323	11.31876
C	7.77258	9.91996	14.59911
H	5.96354	9.80308	13.36877
H	10.93967	9.92134	13.59199
H	7.22435	9.96180	15.56052
N	9.14170	9.95765	14.68611
O	4.99314	5.73807	10.57826
H	4.28858	5.84652	11.26782
H	2.54247	11.53158	10.34083
B	7.05109	9.68663	10.79381
Ti	1.95273	-0.03160	4.88410
Ti	4.87400	-0.02149	4.19308
Ti	7.19495	1.89800	4.92578
Ti	10.10811	1.89800	4.19733
Ti	1.95273	3.82760	4.88410
Ti	1.96603	7.62556	4.95841
Ti	1.96603	11.35444	4.95841
Ti	4.87400	3.81749	4.19308
Ti	4.88673	7.59140	4.26667
Ti	4.88673	11.38860	4.26667
Ti	7.20627	5.69554	4.92413
Ti	7.20629	9.49000	4.96097
Ti	7.20627	13.28446	4.92413
Ti	10.12802	5.69422	4.23725
Ti	10.13103	9.49000	4.28219
Ti	10.12802	13.28578	4.23725
O	1.50815	1.89800	4.85674
O	0.09219	-0.03407	4.08191
O	3.11924	-0.02997	3.25583

O 6.76373 -0.03578 4.87464
O 5.36212 1.89800 4.08511
O 8.34378 1.89800 3.28133
O 1.52660 5.69312 4.91841
O 1.53166 9.49000 4.98906
O 1.52660 13.28688 4.91841
O 0.09219 3.83007 4.08191
O 0.12587 7.62602 4.12486
O 0.12587 11.35398 4.12486
O 3.11924 3.82597 3.25583
O 3.12760 7.62092 3.32997
O 3.12760 11.35908 3.32997
O 6.76373 3.83178 4.87464
O 6.76248 7.62102 4.98540
O 6.76248 11.35898 4.98540
O 5.36629 5.74107 4.08249
O 5.39119 9.49000 4.07365
O 5.36629 13.23893 4.08249
O 8.37288 5.74079 3.29848
O 8.37941 9.49000 3.33900
O 8.37288 13.23921 3.29848

Sample input file for the geometry optimizations using SIESTA 3.1 code.

```
SystemName       L1-anatase101-M
SystemName       L1_M
NumberOfAtoms          110
NumberOfSpecies             5

#--Base
PAO.BasisType split
PAO.BasisSize DZ
PAO.EnergyShift 0.01 eV
PAO.SplitNorm 0.15

MeshCutoff  200.0 Ry

#--Exchange-correlation functionals
XC.functional         GGA
XC.authors            PBE

 ElectronicTemperature           300 K
 MaxSCFIterations                30000
 DM.MixingWeight                 0.02
 DM.NumberPulay                  4
 DM.Tolerance                    1.0D-5
 DM.UseSaveDM                    T

 SolutionMethod                  diagon

 LatticeConstant         1.0000 Ang

%block LatticeVectors
 10.48992200    0.00000000    0.00000000
```

```
 0.00000000   15.18400000    0.00000000
 0.00000000    0.00000000   20.00000000
%endblock LatticeVectors

# K-POINTS
 %block kgrid_Monkhorst_Pack
     1   0   0    0.0
     0   1   0    0.0
     0   0   1    0.0
 %endblock kgrid_Monkhorst_Pack

BandLinesScale          ReciprocalLatticeVectors


MD.TypeOfRun         cg
MD.NumCGsteps        50
MD.MaxCGDispl         0.1  Ang
MD.MaxForceTol        0.04 eV/Ang

WriteCoorXmol   .true.

%block GeometryConstraints
  position from 71 to 110
%endblock GeometryConstraints

%block ChemicalSpeciesLabel
          1          22 Ti
          2           8 O
          3           6 C
          4           1 H
          5           7 N
%endblock ChemicalSpeciesLabel

AtomicCoordinatesFormat  Ang
%block AtomicCoordinatesAndAtomicSpecies
  0.63392  15.30531   8.45636 1
  3.44428   0.08972   7.84637 1
  5.86697   1.97745   8.47463 1
  8.68476   2.03056   7.89409 1
  0.61201   3.91279   8.46258 1
  0.66466   7.73907   8.50505 1
  0.65200  11.50339   8.50068 1
  3.41390   3.85056   7.84803 1
  3.47901   7.74540   7.86787 1
  3.47052  11.49696   7.89325 1
  5.76548   5.73618   8.39093 1
  5.88083   9.60983   8.73694 1
  5.89946  13.40451   8.48108 1
  8.71888   5.87602   7.85821 1
  8.65286   9.64757   7.85534 1
  8.70799  13.41392   7.89856 1
 10.56332   2.04079   8.69353 2
  3.85735   0.02282   5.74898 2
  2.27038  15.34220   9.30666 2
  1.59137  15.24387   6.90091 2
  5.32297  15.30657   8.70379 2
  9.10395   1.94856   5.77415 2
  7.49906   2.03931   9.34539 2
  3.88943   1.97926   7.82948 2
```

```
 6.84180   1.95362   6.92128 2
 9.12118  15.32555   7.92779 2
10.55335   5.81728   8.70492 2
10.62106   9.62047   8.63336 2
10.58386  13.43305   8.70684 2
 3.85291   3.84013   5.74601 2
 3.85726   7.63694   5.82569 2
 3.85871  11.42616   5.82936 2
 2.25176   3.90475   9.31444 2
 2.28527   7.71979   9.36018 2
 2.27971  11.53018   9.36918 2
 1.57656   3.84226   6.90681 2
 1.58951   7.64159   6.94392 2
 1.60967  11.51328   6.95017 2
 5.29851   3.85915   8.71723 2
 5.32874   7.64347   8.51080 2
 5.37930  11.52467   8.61683 2
 9.11158   5.74546   5.82866 2
 9.13154   9.53122   5.83184 2
 9.11208  13.33242   5.80921 2
 7.35865   6.07978   9.44532 2
 7.63130   9.64139   9.39130 2
 7.51526  13.43680   9.36801 2
 3.86195   5.74479   7.84470 2
 3.84832   9.60928   7.94212 2
 3.88315  13.40652   7.93072 2
 6.86495   5.63703   6.95073 2
 6.86345   9.54734   7.02058 2
 6.86285  13.42038   6.93782 2
 9.07369   3.94340   7.95138 2
 9.11805   7.70239   7.94777 2
 9.13344  11.53154   7.93574 2
 6.43325   7.52053  11.40843 2
 5.68446   8.55532  11.59494 3
 5.17367   8.95269  12.95850 3
 5.29919   9.36187  10.60035 2
 5.27922   8.07480  14.06957 3
 4.58099  10.22874  13.16619 3
 4.80924   8.51213  15.33083 3
 5.72446   7.07090  13.94353 4
 4.16169  10.58228  14.47204 3
 4.46292  10.93409  12.32265 4
 4.88038   7.85193  16.21712 4
 3.73124  11.58494  14.67241 4
 4.26493   9.75138  15.55322 5
 7.14026   6.76225  10.26797 4
 1.95273  -0.03160   4.88410 1
 4.87400  -0.02149   4.19308 1
 7.19495   1.89800   4.92578 1
10.10811   1.89800   4.19733 1
 1.95273   3.82760   4.88410 1
 1.96603   7.62556   4.95841 1
 1.96603  11.35444   4.95841 1
 4.87400   3.81749   4.19308 1
 4.88673   7.59140   4.26667 1
 4.88673  11.38860   4.26667 1
 7.20627   5.69554   4.92413 1
 7.20629   9.49000   4.96097 1
 7.20627  13.28446   4.92413 1
```

```
 10.12802   5.69422   4.23725 1
 10.13103   9.49000   4.28219 1
 10.12802  13.28578   4.23725 1
  1.50815   1.89800   4.85674 2
  0.09219  -0.03407   4.08191 2
  3.11924  -0.02997   3.25583 2
  6.76373  -0.03578   4.87464 2
  5.36212   1.89800   4.08511 2
  8.34378   1.89800   3.28133 2
  1.52660   5.69312   4.91841 2
  1.53166   9.49000   4.98906 2
  1.52660  13.28688   4.91841 2
  0.09219   3.83007   4.08191 2
  0.12587   7.62602   4.12486 2
  0.12587  11.35398   4.12486 2
  3.11924   3.82597   3.25583 2
  3.12760   7.62092   3.32997 2
  3.12760  11.35908   3.32997 2
  6.76373   3.83178   4.87464 2
  6.76248   7.62102   4.98540 2
  6.76248  11.35898   4.98540 2
  5.36629   5.74107   4.08249 2
  5.39119   9.49000   4.07365 2
  5.36629  13.23893   4.08249 2
  8.37288   5.74079   3.29848 2
  8.37941   9.49000   3.33900 2
  8.37288  13.23921   3.29848 2
%endblock AtomicCoordinatesAndAtomicSpecies
```

Complete References with more than 10 authors:

Odom, S. A.; Kelley, R. F.; Ohira, S.; Ensley, T. R.; Huang, C.; Padilha, L. A.; Webster, S.; Coropceanu, V.; Barlow, S.; Hagan, D. J.; Van Stryland, E. W.; Bredas, J. L.; Anderson, H. L.; Wasielewski, M. R.; Marder, S. R., Photophysical Properties of an Alkyne-Bridged Bis(zinc porphyrin)-Perylene Bis(dicarboximide) Derivative. *J. Phys. Chem. A* **2009,** *113* (40), 10826-10832.

She, C. X.; Guo, J. C.; Irle, S.; Morokuma, K.; Mohler, D. L.; Zabri, H.; Odobel, F.; Youm, K. T.; Liu, F.; Hupp, J. T.; Lian, T., Comparison of interfacial electron transfer through carboxylate and phosphonate anchoring groups. *J. Phys. Chem. A* **2007,** *111* (29), 6832-6842.

Lin, L. Y.; Tsai, C. H.; Wong, K. T.; Huang, T. W.; Hsieh, L.; Liu, S. H.; Lin, H. W.; Wu, C. C.; Chou, S. H.; Chen, S. H.; Tsai, A. I., "Organic Dyes Containing Coplanar Diphenyl-Substituted Dithienosilole Core for Efficient Dye-Sensitized Solar Cells," *J. Org. Chem.* **2010**, *75*, 4778-4785.

Gaussian 09, Revision C.1, Frisch, M. J.; Trucks, G. W.; Schlegel, H. B.; Scuseria, G. E.; Robb, M. A.; Cheeseman, J. R.; Scalmani, G.; Barone, V.; Mennucci, B.; Petersson, G. A.; Nakatsuji, H.; Caricato, M.; Li, X.; Hratchian, H. P.; Izmaylov, A. F.; Bloino, J.; Zheng, G.; Sonnenberg, J. L.; Hada, M.; Ehara, M.; Toyota, K.; Fukuda, R.; Hasegawa, J.; Ishida, M.; Nakajima, T.; Honda, Y.; Kitao, O.; Nakai, H.; Vreven, T.; Montgomery, Jr., J. A.; Peralta, J. E.; Ogliaro, F.; Bearpark, M.; Heyd, J. J.; Brothers, E.; Kudin, K. N.; Staroverov, V. N.; Kobayashi, R.; Normand, J.; Raghavachari, K.; Rendell, A.; Burant, J. C.; Iyengar, S. S.; Tomasi, J.; Cossi, M.; Rega, N.; Millam, J. M.; Klene, M.; Knox, J. E.; Cross, J. B.; Bakken, V.; Adamo, C.; Jaramillo, J.; Gomperts, R.; Stratmann, R. E.; Yazyev, O.; Austin, A. J.; Cammi, R.; Pomelli, C.; Ochterski, J. W.; Martin, R. L.; Morokuma, K.; Zakrzewski, V. G.; Voth, G. A.; Salvador, P.; Dannenberg, J. J.; Dapprich, S.; Daniels, A. D.; Farkas, Ö.; Foresman, J. B.; Ortiz, J. V.; Cioslowski, J.; Fox, D. J. Gaussian, Inc., Wallingford CT, 2009.